

Convex Relaxations for Isometric and Equiareal NRSfM

Agniva Sengupta, Adrien Bartoli

EnCoV, TGI, Institut Pascal, UMR6602 CNRS, Université Clermont Auvergne, France

agniva.sengupta@uca.fr, adrien.bartoli@gmail.com

Abstract

Extensible objects form a challenging case for Non-Rigid Structure-from-Motion (NRSfM), owing to the lack of a sufficiently constrained extensible model of the point-cloud. We tackle the challenge by proposing 1) convex relaxations of the isometric model up to quasi-isometry, and 2) convex relaxations involving the equiareal deformation model, which preserves local area and has not been used in NRSfM. The equiareal model is appealing because it is physically plausible and widely applicable. However, it has two main difficulties: first, when used on its own, it is ambiguous, and second, it involves quartic, hence highly non-convex, constraints. Our approach handles the first difficulty by mixing the equiareal with the isometric model and the second difficulty by new convex relaxations. We validate our methods on multiple real and synthetic data, including well-known benchmarks.

1. Introduction

Many objects and structures commonly deform. NRSfM is the problem of reconstructing the geometry of such deforming objects from point correspondences across monocular images. NRSfM requires a deformation model, for which the length-preserving isometry is the most common [6, 7, 27]. Consequently, the reconstruction of isometrically deforming surfaces has been well explored and many solutions already exist. However, stretchable surfaces break isometry and defeat these methods. In contrast, the area-preserving equiareal model is obeyed by many real-world stretchable objects and hence, offers a valuable alternative to isometry. We propose models and methods for NRSfM that allow significant deviation from isometry, in the form of: 1) deviation from the isometric solution up to some tolerance, and 2) deviation from the isometric solution while following the equiareal model as closely as possible.

Existing methods for Non-Rigid Structure-from-Motion (NRSfM) are broadly split into two categories, depending on the type of deformation model they use: *i)* Low Rank Shape Basis (LRSB) [9, 12, 17, 18], and *ii)* physics-based or

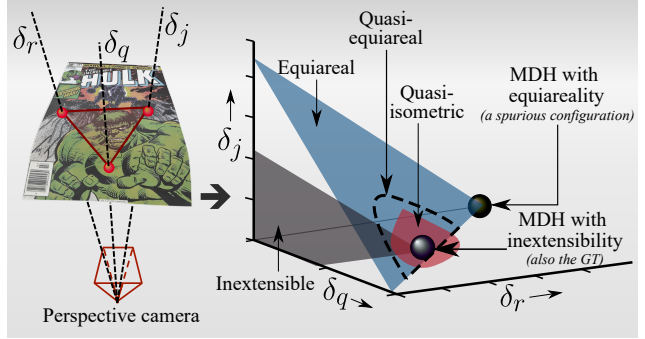


Figure 1. Observation of the solution spaces for three simulated points in general configuration observed by a perspective camera and parameterised by their depths δ_j , δ_q , and δ_r . The *Gt* point is in the centre. The solution spaces for inextensibility and equiareality are unbounded subspaces. Using the MDH with inextensibility yields a solution point reasonably close to the *Gt*. However, using the MDH with equiareality yields a spurious solution point. The proposed quasi-isometric and quasi-equiareal formulations are smaller bounded subspaces enclosing the *Gt*.

differential models. The latter type was solved from point correspondences [8], the so-called *zeroth-order methods*, and their derivatives [21, 23]. Isometric NRSfM received solutions based on convex relaxations with the zeroth-order methods [8, 15]. These solutions use the Maximum Depth Heuristic (MDH) with inextensibility constraints. The angle-preserving conformal deformation model was also investigated [22] but shows very limited applicability to real-world objects. In contrast, equiareality has never been explored. A possible reason is the inherent intractability of the problem [11]. Interestingly however, the area of simplices bounded by sightlines can be expressed as polynomials which can be reparameterised and relaxed to convex formulations. Our proposed approaches search the near vicinity of the solution space of MDH - isometric NRSfM, either freely up to a tolerance, or using equiareality as a secondary objective. Figure (1) illustrates the intuition behind this reasoning.

Technically, our *first* contribution is to reformulate isometric NRSfM with a more restrictive relaxation than any

other previous approaches, yielding a strictly isometric method. Our *second* contribution is to relax this strict isometry up to a defined tolerance which, unlike the well-known inextensibility, is not restricted to a convex cone. Our *third* contribution is to parameterise the solutions using 3D point positions in \mathbb{R}^3 , instead of the prevalent noise-sensitive Depth-Along-Sight-Lines (DaSL). Our *fourth* contribution is the introduction of a deformation model combining isometry and equiareality. In addition, we establish the close relationship of NRSfM to the Graph Realisation Problem (GRP) and show how the two fields can cross-fertilise. All our methods are solved with convex optimisation. They reconstruct benchmark datasets with state-of-the-art accuracy and stretchable surfaces with an accuracy unmatched by any other NRSfM method.

2. Background

We describe the NRSfM literature and background.

NRSfM. NRSfM has been essentially dealt with using isometry [6, 7, 21, 25]. Following early work on Shape-from-Template (SfT) [25], which showed that isometry leads to surface flipping ambiguities, heuristics were proposed to force a unique solution, MDH being the most prominent [28]. NRSfM has also been addressed using the conformal model [22]. In contrast, equiareality is highly ambiguous as a deformation constraint [10, 11]. An earlier attempt to solve equiareal NRSfM concluded on its impossibility [22]. Indeed, an equiareally deforming surface has more independent parameters than the number of constraints it generates. Later, a hybrid equiareal NRSfM was attempted [23], but with lower accuracy than isometric and conformity. Interestingly, [5] attempted to solve the closely related and better constrained SfT problem with equiareality; it concluded that even equiareal SfT is unsolvable without additional priors in the form of boundary conditions. To date, no convex formulation to equiareal NRSfM has been known.

Convex solutions to NRSfM. To solve the NRSfM problem, [8] proposed convex inextensibility relaxations. The squared Euclidean distance between points in \mathbb{R}^3 can be trivially obtained as a quadratic function. The inextensible model upper bounds the Euclidean distance up to an unknown geodesic distance. Such inequality constraints in the Lorentz cone of quadratic terms form a special subclass of conic optimisation, Second-Order Cone Programming (SOCP). [15] realised that a reformulation of inextensibility constraints allow the Euclidean distances between point-pairs to be restricted to semidefinite cones, hence posed the problem as an Semi-Definite Programming (SDP) and a trace minimisation of these SDP matrices (as a convex surrogate for rank) of depth-of-points. This also has the desirable side-effect of maximising rigidity.

Existing approaches do not deal with the unrelaxed, original isometry constraint, nor with the equiareal constraint. They all follow inextensibility and rely on an Nearest-Neighborhood Graph (NNG) to impart a graph structure to the input point correspondences. Isometric NRSfM is therefore the problem of finding the most isometric configuration of the NNG in \mathbb{R}^3 , subject to additional constraints, including reprojection and surface smoothness. This formulation compels comparison with GRP [2], which has many applications in fields including wireless sensor network localisation, molecular conformation, design and analysis of tensegrity structures.

Graph realisation problem. We consider a set of n vertices $\{\mathbf{v}_i \in \mathbb{R}^d\}$, $i \in [1, n]$, with a prescribed Euclidean Distance Matrix (EDM) denoted by $\mathbf{D} \in \mathbb{R}^{n \times n}$ such that $\mathbf{D}_{i,i'} = \|\mathbf{v}_i - \mathbf{v}_{i'}\|$. For an adjacency matrix \mathcal{E} imparting a graph structure on $\{\mathbf{v}_i\}$, the problem of recovering the unknown vertex positions $\{\mathbf{v}_i\}$ from a sparse but known EDM forms the Anchor-Free Graph Realization Problem (AF-G-RP). The wireless sensor network localisation literature [29] offers a well-known SDP solution to AF-G-RP. A Gram Matrix (GM) obtained from the vertex positions as $\mathbf{Y} = \mathbf{v}\mathbf{v}^\top$, where $\mathbf{v}^\top = (\mathbf{v}_1^\top, \dots, \mathbf{v}_n^\top)$ parameterises the SDP. Given a sparse observation of some elements of \mathbf{Y} , attempting to reduce the rank of \mathbf{Y} while maintaining it as Positive Semi-definite (PSD) performs *matrix completion* [4]. Matrix completion by SDP is a well-studied problem. There exists a linear expression in \mathbf{Y} for the Euclidean distance between vertices. Combining the matrix completion via SDP with this linear expression yields:

$$\min_{\mathbf{Y}} \text{tr}(\mathbf{Y}) \quad (1a)$$

$$\text{s.t.} \quad \mathbf{Y}_{i,i} + \mathbf{Y}_{i',i'} - 2\mathbf{Y}_{i,i'} = \mathbf{D}_{i,i'}, \quad (1b)$$

$$\mathbf{Y} \in \mathbf{S}_+^n, \quad \forall i, i' \in [1, n]. \quad (1c)$$

A solution to equation (1) forms the *Biswas-Ye Semidefinite Relaxation* solutions to AF-G-RP problem [3]. There also exists variants of equation (1) where only the upper and/or lower bounds of the Euclidean distances in \mathbf{D} can be observed, e.g., in *molecular conformation*.

Beyond Euclidean distances. The linearisation of Euclidean distances in equation (1b) happens due to ‘lifting’ the solution to a higher-dimensional space (higher-rank SDP). However, from the theory of *polynomial optimisation*, there exists well-known methods to solve any global unconstrained minimisation of a Sum-of-Squares (SoS) polynomial by a finite sequence of Linear Matrix Inequality (LMI) relaxations [20]. Therefore, the approximation of Euclidean distances, as in equation (1b), is just one possible variant of polynomial valued function linearised using a higher dimensional PSD matrix. Such an approach

had indeed already been used for solving first-order, isometric NRSfM [26]. Interestingly, the experiments of [26] point to the discretionary nature of the higher degree LMI relaxations for the NRSfM problem. Another possibility is to formulate constraints based on angle between vertices, as in the *angle based sensor network localisation* problem [16]. Importantly, equiareal constraints have never been handled using SDP in the context of computer vision or otherwise.

3. Methods

We describe our NRSfM methods in details.

3.1. Notation and Preliminaries

NRSfM takes as inputs m point correspondences across n images taken from a perspective camera with known intrinsics. The point correspondences are denoted by their normalised homogeneous coordinates $\{\mathbf{x}_i = (\mathbf{p}_{i,1}, \dots, \mathbf{p}_{i,m})^\top \in \mathbb{R}^{m \times 3}\}$, $i \in [1, n]$, and corresponding unknown 3D points by $\{\mathbf{X}_i = (\mathbf{P}_{i,1}, \dots, \mathbf{P}_{i,m})^\top \in \mathbb{R}^{m \times 3}\}$, $i \in [1, n]$. $\mathbf{P}_{i,j} = (X_{i,j}, Y_{i,j}, Z_{i,j})^\top$ is linked to $\mathbf{p}_{i,j}$ by the perspective projection function $\Pi(\mathbf{P}_{i,j}) = \mathbf{p}_{i,j} = \mathbf{P}_{i,j}/Z_{i,j}$. The Sight-Line (SL) is the line directed along $\mathbf{d}_{i,j} \in S^2$ passing through the camera centre such that $\mathbf{d}_{i,j} = \mathbf{p}_{i,j}/\|\mathbf{p}_{i,j}\| = (x_{i,j}, y_{i,j}, z_{i,j})^\top$. Each \mathbf{X}_i lies on the surface embedding $\mathcal{S}_i \subset \mathbb{R}^3$ which is linked to an unknown parameterisation $\mathcal{T} \subset \mathbb{R}^2$. For isometric deformations, *geodesic distances* along the surface manifold \mathcal{S}_i must be preserved, while for equiareal deformations, area on the surface manifold \mathcal{S}_i must be preserved.

We denote as \mathcal{E} , the set of edges of a fully connected graph with points in \mathbf{x}_1 as vertices. From \mathcal{E} , we derive the following: 1) a set of 1-simplices $\mathcal{E}_2 \subset \mathcal{E}$, and 2) a set of 2-simplices $\mathcal{E}_3 = \{(j, q, r)\}$, where $(j, q), (q, r), (r, j) \in \mathcal{E}_2$, such that $(\mathbf{P}_{i,j}, \mathbf{P}_{i,q}, \mathbf{P}_{i,r})$ forms a 2-simplex. We define $|\mathcal{E}_2| = p_1$ and $|\mathcal{E}_3| = p_2$. We define two more sets \mathcal{G}_2 and \mathcal{G}_3 , such that: 1) \mathcal{G}_2 is the set of geodesic distances for all 1-simplices in \mathcal{E}_2 , and 2) \mathcal{G}_3 is the set of areas for all 2-simplices in \mathcal{E}_3 . For NRSfM, \mathcal{G}_2 and \mathcal{G}_3 are unknowns. We define two functions: 1) $\mathbf{g}_I(i, j, q)$ computes the distance between $\mathbf{P}_{i,j}$ and $\mathbf{P}_{i,q}$ and 2) $\mathbf{g}_E(i, j, q, r)$ computes the area of the triangle with $\mathbf{P}_{i,j}$, $\mathbf{P}_{i,q}$ and $\mathbf{P}_{i,r}$ as vertices in \mathbb{R}^3 . We denote by \mathbf{S}_+^n the group of $n \times n$ dimensional PSD matrices. We use the notation $\sum_{i_1=1}^{x_1} \dots \sum_{i_z=1}^{x_z}$ to denote the z -times summation $\sum_{i_1=1}^{x_1} \sum_{i_2=1}^{x_2} \dots \sum_{i_z=1}^{x_z}$.

3.2. Problem Statement

We assume \mathcal{E}_2 and \mathcal{E}_3 are given and we solve the NRSfM problem using isometric and equiareal constraints. We do so by solving three different variants, two involving just isometry and one involving equiareality. Isometric NRSfM does not possess a unique solution without additional priors,

MDH being the most widely used. This is implemented as a depth-maximisation term added to the cost, denoted by f_{mdh} . For equiareal NRSfM, we observe the following:

Lemma 1. *There does not exist a unique solution, even up to scale, for zeroth-order NRSfM using just equiareal and reprojection constraints.*

Proof. Section 1 of supplementary materials¹. \square

Unfortunately, MDH is not a valid prior for equiareal NRSfM. Therefore, equiareal NRSfM requires other additional constraints and priors. The problem we actually solve is a hybrid-equiareal NRSfM with a quasi-isometric cost weighted down to allow significant deviation from isometry, maintaining perfect equiareality between corresponding 2-simplices.

To describe our problem statement, we introduce two cost functions: *i*) a cost for MDH $f_{\text{mdh}}(\mathbf{X}_i)$, the maximisation of which increases the depth of \mathbf{X}_i along the positive Z axis in \mathbb{R}^3 , and *ii*) a reprojection cost $f_{\text{prj}}(\mathbf{X}_i, \mathbf{x}_i)$ which penalises deviation of $\Pi(\mathbf{P}_{i,j})$ from $\mathbf{p}_{i,j}$ for $i \in [1, n], j \in [1, m]$. Our problem statements are:

1) Strictly Isometric NRSfM (sI-NRSfM):

$$\{\mathbf{X}_i\}, \mathcal{G}_2 = \underset{\{\mathbf{X}_i\}, \mathcal{G}_2}{\operatorname{argmin}} \sum_{i=1}^n \left(f_{\text{prj}}(\mathbf{X}_i, \mathbf{x}_i) - f_{\text{mdh}}(\mathbf{X}_i) \right) \quad (2a)$$

$$\text{s.t. } \mathbf{g}_I(i, j, q) = \mathcal{G}_2(j, q), \quad (2b)$$

$$\forall \quad i \in [1, n], \quad j, q \in [1, m], \quad (j, q) \in \mathcal{E}_2. \quad (2c)$$

2) Quasi Isometric NRSfM (qI-NRSfM):

$$\begin{aligned} \{\mathbf{X}_i\}, \mathcal{G}_2 = \underset{\{\mathbf{X}_i\}, \mathcal{G}_2}{\operatorname{argmin}} & \sum_{i,j,q=1}^{n,m,\mathcal{E}_2(j)} |\mathbf{g}_I(i, j, q) - \mathcal{G}_2(j, q)| \\ & + \sum_{i=1}^n \left(f_{\text{prj}}(\mathbf{X}_i, \mathbf{x}_i) - f_{\text{mdh}}(\mathbf{X}_i) \right) \end{aligned} \quad (3a)$$

$$\forall \quad i \in [1, n], \quad j, q \in [1, m], \quad (j, q) \in \mathcal{E}_2. \quad (3b)$$

3) Quasi Equiareal NRSfM (qE-NRSfM):

$$\begin{aligned} \{\mathbf{X}_i\}, \mathcal{G}_2, \mathcal{G}_3 = \underset{\{\mathbf{X}_i\}, \mathcal{G}_2, \mathcal{G}_3}{\operatorname{argmin}} & \left(f_{\text{prj}}(\mathbf{X}_i, \mathbf{x}_i) - f_{\text{mdh}}(\mathbf{X}_i) \right) \\ & + \lambda_I \sum_{i,j,q=1}^{n,m,\mathcal{E}_2(j)} |\mathbf{g}_I(i, j, q) - \mathcal{G}_2(j, q)| \\ & + \lambda_E \sum_{i,j,q,r=1}^{n,m,\mathcal{E}_2(j), \mathcal{E}_3(j,q)} |\mathbf{g}_E(i, j, q, r) - \mathcal{G}_3(j, q, r)| \end{aligned} \quad (4a)$$

$$\forall \quad i \in [1, n], \quad j, q, r \in [1, m], \quad (j, q, r) \in \mathcal{E}_3. \quad (4b)$$

Beyond these formulations, our technical contributions are reparameterisations and convex relaxation to sI-NRSfM and qI-NRSfM in section 3.3 and to qE-NRSfM in section 3.4.

¹Supplementary materials appended at the end of this document

3.3. Isometric Cost: Relaxation, Convex Reparameterisation and Isometric Methods

The next two sections give our isometric methods. The first set of methods uses the DaSL parameterisation, where an unknown point $\mathbf{P}_{i,j}$ is parameterised by its depth along its SL $\mathbf{d}_{i,j}$, as in existing work. The second set of methods uses the Position in \mathbb{R}^3 ($p3D$) parameterisation, where $\mathbf{P}_{i,j}$ may not lie on $\mathbf{d}_{i,j}$ exactly. Importantly, using $p3D$ allows us to handle correspondence noise must better than DaSL.

3.3.1 Parameterisation with DaSL

The DaSL parameterisation defines $\mathbf{P}_{i,j} = \delta_{i,j} \mathbf{d}_{i,j}$ for depth $\delta_{i,j} \in \mathbb{R}_+$. Stacked together for the i -th image, the depth vector is $\mathbf{d}_i^\top = (\delta_{i,1}, \dots, \delta_{i,m})$. We define the Depth Gram Matrix (DGM) as $\mathfrak{R}_i = \mathbf{d}_i \mathbf{d}_i^\top$, which is related to the Euclidean distances by:

$$\mathbf{g}_I^\delta(i, j, q) = \mathfrak{R}_{i,j,j} + \mathfrak{R}_{i,q,q} - 2\mathfrak{R}_{i,j,q} \langle \mathbf{d}_{i,j}, \mathbf{d}_{i,q} \rangle, \quad (5)$$

where $\mathbf{g}_I^\delta(i, j, q)$ is the implementation of \mathbf{g}_I for DaSL. Therefore, we express equation (2) parameterised by DGM and $\mathbf{g}_I^\delta(i, j, q)$ as equation (5). To handle the global scale ambiguity, we require the geodesics to sum to 1. Moreover, DGM has to be PSD and of rank 1. However, strict rank restrictions being non-convex, we use the common convex relaxation provided by trace minimisation of \mathfrak{R}_i . Eventually, we implement $f_{\text{mdh}}(\mathbf{X}_i)$ by the minimisation of the inverse diagonal elements of \mathfrak{R}_i , whilst f_{prj} is already enforced by DaSL. Therefore, our final solution to $sI\text{-NRSfM}$ parameterised by DaSL is:

$$\min_{\{\mathfrak{R}_i\}, \mathcal{G}_2} \sum_{i=1}^n \text{tr}(\mathfrak{R}_i) + \sum_{i,j=1}^{n,m} \frac{1}{\mathfrak{R}_{i,j,j}} \quad (6a)$$

s.t.

$$\mathbf{g}_I^\delta(i, j, q) = \mathcal{G}_2(j, q), \quad \sum_{j,q=1}^{m, \mathcal{E}_2(j)} \mathcal{G}_2(j, q) = 1,$$

$$\mathfrak{R}_i \in \mathbf{S}_+^m, \quad \forall \quad i \in [1, n], j \in [1, m], (j, q) \in \mathcal{E}_2, \quad (6b)$$

which is a convex formulation solved by standard SDP.

We modify equation (6a)-(6b) to solve $qI\text{-NRSfM}$ by recasting it in Lagrangian form, modifying the strict equality in equation (6b) to an ℓ^1 -norm minimisation, giving the DaSL solution to $qI\text{-NRSfM}$:

$$\min_{\{\mathfrak{R}_i\}, \mathcal{G}_2} \sum_{i=1}^n \text{tr}(\mathfrak{R}_i) + \sum_{i,j=1}^{n,m} \frac{1}{\mathfrak{R}_{i,j,j}} + \lambda_I \sum_{i,j,q=1}^{n,m, \mathcal{E}_2(j)} \left(|\mathbf{g}_I^\delta(i, j, q) - \mathcal{G}_2(j, q)| \right), \quad (7a)$$

$$\text{s.t.} \quad \sum_{j,q=1}^{m, \mathcal{E}_2(j)} \mathcal{G}_2(j, q) = 1, \quad \mathfrak{R}_i \in \mathbf{S}_+^m, \quad (7b)$$

$$\forall \quad i \in [1, n], \quad j \in [1, m], \quad (j, q) \in \mathcal{E}_2. \quad (7c)$$

3.3.2 Parameterisation with $p3D$

The $p3D$ parameterisation directly uses $\mathbf{P}_{i,j} \in \mathbb{R}^3$. Stacked together for the i -th image, the position vector is $\mathfrak{P}_i^\top = (\mathbf{P}_{i,1}^\top, \dots, \mathbf{P}_{i,m}^\top) \in \mathbb{R}^{3m}$. We define the Position Gram Matrix (PGM) as $\mathfrak{S}_i = \mathfrak{P}_i \mathfrak{P}_i^\top$, which is related to the Euclidean distances by:

$$\mathbf{g}_I^P(i, j, q) = \|\mathbf{P}_{i,j} - \mathbf{P}_{i,q}\|_2^2 = \mathfrak{S}_{i,j_x,j_x} + \mathfrak{S}_{i,j_y,j_y} + \mathfrak{S}_{i,j_z,j_z} + \mathfrak{S}_{i,q_x,q_x} + \mathfrak{S}_{i,q_y,q_y} + \mathfrak{S}_{i,q_z,q_z} - 2(\mathfrak{S}_{i,j_x,q_x} + \mathfrak{S}_{i,j_y,q_y} + \mathfrak{S}_{i,j_z,q_z}), \quad (8)$$

where $(j_x, j_y, j_z) = 3(j-1) + (1, 2, 3)$ and (q_x, q_y, q_z) are also obtained similarly. We formulate the reprojection cost f_{prj} for $sI\text{-NRSfM}$ and $qI\text{-NRSfM}$ as $f_{i,j}^\Pi$, given by:

$$f_{i,j}^\Pi(\mathfrak{S}_i) = \|\mathbf{P}_{i,j} \times \mathbf{d}_{i,j}\|_2^2 = \mathfrak{S}_{i,j_x,j_x} (y_{i,j}^2 + z_{i,j}^2) + \mathfrak{S}_{i,j_y,j_y} (x_{i,j}^2 + z_{i,j}^2) + \mathfrak{S}_{i,j_z,j_z} (x_{i,j}^2 + y_{i,j}^2) - 2(\mathfrak{S}_{i,j_x,j_y} x_{i,j} y_{i,j} + \mathfrak{S}_{i,j_x,j_z} x_{i,j} z_{i,j} + \mathfrak{S}_{i,j_y,j_z} y_{i,j} z_{i,j}). \quad (9)$$

Adapting MDH to $p3D$ is non-trivial, as it requires the Z -component of $\mathbf{P}_{i,j}$ to be in \mathbb{R}_+ whilst the X and Y components should be left free in \mathbb{R} . This is not realisable on a PGM which is being used as the unknown parameter. To resolve this, we augment the PGM with an additional row and column as:

$$\mathfrak{S}'_i = \begin{pmatrix} 1 & \mathfrak{P}_i^\top \\ \mathfrak{P}_i & \mathfrak{S}_i \end{pmatrix}, \quad (10)$$

which also happens to be the moment matrix of first order LMI relaxation [19]. The first column or row of \mathfrak{S}'_i allows us to compute $\langle \mathbf{P}_{i,j}, \mathbf{d}_{i,j} \rangle$, which is a signed scalar value. Hence, maximising $\langle \mathbf{P}_{i,j}, \mathbf{d}_{i,j} \rangle$ ensures non-negative $Z_{i,j}$. The MDH cost function f_{mdh} for $p3D$ is then given as:

$$f_{i,j}^\delta(\mathfrak{S}'_i) = \left(\mathfrak{S}'_{i,j'_x,1}, \mathfrak{S}'_{i,j'_y,1}, \mathfrak{S}'_{i,j'_z,1} \right)^\top \mathbf{d}_{i,j}. \quad (11)$$

where $(j'_x, j'_y, j'_z) = (j_x, j_y, j_z) + 1$ due to equation (10). With a slight abuse of notation, we consider these change of indices to be transmitted appropriately to $f_{i,j}^\Pi(\mathfrak{S}'_i)$ and $\mathbf{g}_I^P(i, j, q)$.

In order to solve $sI\text{-NRSfM}$ with $p3D$, we *i*) reparameterise equation (2) with \mathfrak{S}'_i , *ii*) introduce MDH by maximising $\langle \mathbf{P}_{i,j}, \mathbf{d}_{i,j} \rangle$, *iii*) anchor the scale of the scene by requiring \mathcal{G}_2 to sum to 1, and *iv*) relax exact rank constraint on \mathfrak{S}'_i to minimise $\text{tr}(\mathfrak{S}'_i)$, i.e., an exact $p3D$ counterpart of the

DaSL solution in equation (6a)-(6b) with an additional re-projection error. Therefore, the $p3D$ solution to sI -NRSfM is:

$$\min_{\{\mathcal{S}'_i\}, \mathcal{G}_2} \sum_{i=1}^n \text{tr}(\mathcal{S}'_i) + \sum_{i,j=1}^{n,m} f_{i,j}^\Pi(\mathcal{S}'_i) - \sum_{i,j=1}^{n,m} f_{i,j}^\delta(\mathcal{S}'_i) \quad (12a)$$

$$\text{s.t. } \mathcal{G}_2(j, q) = \mathbf{g}_I^P(i, j, q),$$

$$\sum_{j,q=1}^{m, \mathcal{E}_2(j)} \mathcal{G}_2(j, q) = 1, \mathcal{S}'_{i,1,1} = 1, \mathcal{S}'_i \in \mathbf{S}_+^{m+1} \quad (12b)$$

$$\forall i \in [1, n], j \in [1, m], (j, q) \in \mathcal{E}_2. \quad (12c)$$

The $p3D$ solution for qI -NRSfM is:

$$\min_{\{\mathcal{S}'_i\}, \mathcal{G}_2} \left(\sum_{i=1}^n \text{tr}(\mathcal{S}'_i) + \sum_{i,j,q=1}^{n,m, \mathcal{E}_2(j)} \left(f_{i,j}^\Pi(\mathcal{S}'_i) + \lambda_I |\mathbf{g}_I^P(i, j, q) - \mathcal{G}_2(j, q) - f_{i,j}^\delta(\mathcal{S}'_i)| \right) \right) \quad (13a)$$

$$\text{s.t. } \sum_{j,q=1}^{m, \mathcal{E}_2(j)} \mathcal{G}_2(j, q) = 1, \mathcal{S}'_{i,1,1} = 1, \mathcal{S}'_i \in \mathbf{S}_+^{m+1} \quad (13b)$$

$$\forall i \in [1, n], j \in [1, m], (j, q) \in \mathcal{E}_2. \quad (13c)$$

Again, equations (12) and (13) represent convex problems solvable by standard SDP.

Correspondence completion. In addition to dealing with noise, $p3D$ allows one to implement correspondence completion. In the vast majority of cases, the input correspondences $\{\mathbf{x}_i\}$ have missing points. We write the visibility indicator as \mathcal{V} such that $\mathcal{V}_{i,j} = 1$ if $\mathbf{p}_{i,j}$ is visible and 0 otherwise. Existing isometric methods handle incomplete data, but do not hallucinate the missing points. To all such missing points in \mathcal{N}'_i , we assign s Proximal Neighbors (PN) which are its s closest neighbours in \mathbf{x}_1 . We guide the depth maximisation of these invisible points with the support of SL from its PN, leaving the rest of the minimisation as is for both sI -NRSfM and qI -NRSfM. The SDP solution computes the position in \mathbb{R}^3 for these missing vertices, as if ‘hallucinating’ correspondences that are not part of the inputs. We do this by substituting the scalar product $f_{i,j}^\delta(\mathcal{S}'_i)$ in equations (12a) and (13a) by a function $g_{i,j}^\delta(\mathcal{S}'_i)$, which when evaluated for the (i, j) -th point is written as:

$$g_{i,j}^\delta(\mathcal{S}'_i) = \begin{cases} \left(\mathcal{S}'_{i,j'_x,1}, \mathcal{S}'_{i,j'_y,1}, \mathcal{S}'_{i,j'_z,1} \right)^\top \mathbf{d}_{i,j} & \text{if } \mathcal{V}_{i,j} = 1, \\ \sum_{l=1}^{\text{PN}(j)} \left(\mathcal{S}'_{i,j'_x,1}, \mathcal{S}'_{i,j'_y,1}, \mathcal{S}'_{i,j'_z,1} \right)^\top \mathbf{d}_{i,l} & \text{otherwise.} \end{cases} \quad (14)$$

3.4. Equiareal Cost: Convex Relaxations and Quasi-equiareality

We describe our method to solve qE -NRSfM by first computing \mathbf{g}_E^δ and \mathbf{g}_E^P followed by convex relaxations to linearise these two functions.

Area of 2-simplices. We observe that the square area enclosed by vertices $\mathbf{P}_{i,j}, \mathbf{P}_{i,q}, \mathbf{P}_{i,r} \in \mathbf{X}_i$ can be expressed as a quartic with both DaSL and $p3D$ parameterisations. For $(\mathbf{P}_{i,j}, \mathbf{P}_{i,q}, \mathbf{P}_{i,r})$, the square area using DaSL parameterisation is expressed by a function $h_E^\delta(i, j, q, r)$ which is a trivariate quartic in $\delta_{i,j}, \delta_{i,q}$ and $\delta_{i,r}$. Similarly expanding the square area for $p3D$ results in a function $h_E^P(i, j, q, r)$ which, when expanded element-wise, also results in a quartic in the 9 coordinates of $\mathbf{P}_{i,j}, \mathbf{P}_{i,q}$ and $\mathbf{P}_{i,r}$. The detailed expressions are given in section (2) of supplementary materials.

Sparsity-aware convex relaxations for h_E^δ and h_E^P . There exists a well-known technique for convex relaxations of multivariate polynomials, namely, Lasserre’s hierarchy of LMI Relaxations (LhLR) [19]. However, standard LhLR would require full moment matrices for second order relaxations in order to arrive at a linear expression for multivariate quartics, which are highly computationally expensive. However, we show the following:

Proposition 1. *For the i -th image, h_E^δ and h_E^P admits lower-degree relaxations using sub-matrices of second-order moment matrices of LhLR, given by $\mathfrak{T}_i \in \mathbf{S}_+^{\tilde{p}_2+m}$ and $\mathfrak{U}_i \in \mathbf{S}_+^{6\tilde{p}_2+3m+1}$ respectively, where \tilde{p}_2 are the number of unique edges of the 2-simplices in \mathcal{E}_3*

Proof. We define two vectors \mathfrak{E}_i and \mathfrak{Q}_i as:

$$\begin{aligned} \mathfrak{E}_i^\top &= (\delta_{i,1}, \dots, \delta_{i,m}, \dots, \delta_{i,j}\delta_{i,q}, \delta_{i,q}\delta_{i,r}, \delta_{i,j}\delta_{i,r}, \dots), \\ \mathfrak{Q}_i^\top &= (1, \mathbf{P}_{i,1}^\top, \dots, \mathbf{P}_{i,m}^\top, \dots, \vartheta(i, j, q)^\top, \vartheta(i, q, r)^\top, \\ &\quad \vartheta(i, j, r)^\top, \dots), \quad \forall (j, q, r) \in \mathcal{E}_3, \end{aligned} \quad (15)$$

such that:

$$\vartheta(i, j, q)^\top = (X_{i,j}Y_{i,q}, X_{i,j}Z_{i,q}, Y_{i,j}X_{i,q}, Y_{i,j}Z_{i,q}, Z_{i,j}X_{i,q}, Z_{i,j}Y_{i,q}). \quad (16)$$

This allows us to construct two augmented Gram matrices, $\mathfrak{T}_i = \mathfrak{E}_i \mathfrak{E}_i^\top$ and $\mathfrak{U}_i = \mathfrak{Q}_i \mathfrak{Q}_i^\top$. We show that \mathfrak{T}_i and \mathfrak{U}_i are sufficient to express the quartics in h_E^δ and h_E^P respectively as a linear combination of their elements. Let $\mathbf{g}_E^\delta(i, j, q, r)$ and $\mathbf{g}_E^P(i, j, q, r)$ be functions that maps $(\mathbf{P}_{i,j}, \mathbf{P}_{i,q}, \mathbf{P}_{i,r})$ to their area using linear combinations of elements from \mathfrak{T}_i and \mathfrak{U}_i respectively. We define

two maps: a) $\Omega^k : \mathbb{Z}^3 \mapsto \mathbb{Z}^3$ such that $\Omega^k(j, q, r) = (a_1, a_2, a_3)$ and $\mathfrak{T}_{i,a_1,a_1} = \delta_{i,j}^2 \delta_{i,q}^2$, $\mathfrak{T}_{i,a_2,a_2} = \delta_{i,q}^2 \delta_{i,r}^2$, and $\mathfrak{T}_{i,a_3,a_3} = \delta_{i,j}^2 \delta_{i,r}^2$, and b) $\rho^k : \mathbb{Z}^3 \mapsto \mathbb{Z}^{18}$ such that $\rho^k(j, q, r) = (b_1, \dots, b_{18})$ and the following set of identities apply: $\{\mathfrak{U}_{i,b_1,b_1} = X_{i,j}^2 Y_{i,q}^2, \dots, \mathfrak{U}_{i,b_{18},b_{18}} = Z_{i,r}^2 Y_{i,q}^2\}$. The details are given in section (3) of supplementary materials for \mathfrak{g}_E^δ and \mathfrak{g}_E^P . \square

Localised constraints on \mathfrak{T}_i and \mathfrak{U}_i . Some of the diagonal elements of \mathfrak{T}_i and \mathfrak{U}_i are equal to some other squared off-diagonal elements of themselves and this mapping is obtainable from Ω^k and ρ^k . However, the equality between an element of a matrix with another squared element of itself is non-affine, hence non-convex. So we relax it to an inequality constraint in the convex cone of the squared term, i.e., for $(j, q) \leftrightarrow a_1$, we change the constraint $\mathfrak{T}_{i,j,q}^2 = \mathfrak{T}_{i,a_1,a_1}$ to $\mathfrak{T}_{i,j,q}^2 \leq \mathfrak{T}_{i,a_1,a_1}$. This is combined with minimisation of the traces of \mathfrak{T}_i and \mathfrak{U}_i while maximising depth. With an appropriate (λ_I, λ_E) (from the qE -NRSfM problem statement), this relaxation finds an accurate solution that slightly violates isometry of 1-simplices while maintaining equiareality of 2-simplices.

3.4.1 Parameterisation with DaSL

We follow four steps to solve qE -NRSfM with DaSL: *i)* we do all the convex relaxations, reparameterisation and inclusion of MDH as in equation (7), *ii)* we relax the exact rank-1 constraint on \mathfrak{T}_i to trace minimisation, *iii)* we minimise the ℓ^1 -norm of the difference between the areas of all 2-simplices in \mathcal{E}_3 and the estimated areas in $\mathcal{G}_3(j, q, r)$, and *iv)* we impose inequality constraints between elements of \mathfrak{T}_i . With these modifications, qE -NRSfM is expressed as:

$$\begin{aligned} \min_{\{\mathfrak{T}_i\}, \mathcal{G}_2, \mathcal{G}_3} & \sum_{i=1}^n \text{tr}(\mathfrak{T}_i) + \sum_{i,j,q=1}^{n,m,\mathcal{E}_2(j)} \lambda_I \left(|\mathfrak{g}_I^\delta(i, j, q) - \mathcal{G}_2(j, q)| \right) \\ & + \sum_{i,j=1}^{n,m} \left(\frac{1}{\mathfrak{T}_{i,j,j}} + \sum_{q,r=1}^{\mathcal{E}_2(j), \mathcal{E}_3(j,q)} \lambda_E |\mathfrak{g}_E^\delta(i, j, q, r) - \mathcal{G}_3(j, q, r)| \right), \end{aligned} \quad (17a)$$

$$\text{s.t. } \mathfrak{T}_{i,j,q}^2 \leq \mathfrak{T}_{i,a_1,a_1}, \mathfrak{T}_{i,q,r} \leq \mathfrak{T}_{i,a_2,a_2}, \mathfrak{T}_{i,j,r} \leq \mathfrak{T}_{i,a_3,a_3}, \quad (17b)$$

$$\sum_{j,q=1}^{m,\mathcal{E}_2(j)} \mathcal{G}_2(j, q) = 1, \mathfrak{T}_i \in \mathbf{S}_+^{\tilde{p}_2+m} \quad \forall i \in [i, n], j \in [1, m], \quad (17c)$$

$$(j, q) \in \mathcal{E}_2, (j, q, r) \in \mathcal{E}_3, (a_1, a_2, a_3) \in \Omega^k(j, q, r), \lambda_I > 0. \quad (17d)$$

3.4.2 Parameterisation with p3D

We follow four steps to solve qE -NRSfM with p3D: *i)* we do all the convex relaxations, reparameterisation and inclu-

sion of MDH as in equation (13), *ii)* we relax the exact rank-1 constraint on \mathfrak{U}_i to trace minimisation, *iii)* we minimise area difference, as in equation (17a), and *iv)* we impose inequality constraints between diagonal and off-diagonal elements of \mathfrak{U}_i . We obtain the following solution:

$$\begin{aligned} \min_{\{\mathfrak{U}_i\}, \mathcal{G}_2, \mathcal{G}_3} & \sum_{i=1}^n \left(\left(f_{i,j}^\Pi(\mathfrak{S}'_i) + \text{tr}(\mathfrak{U}_i) \right) + \sum_{j,q=1}^{m,\mathcal{E}_2(j)} \left(\lambda_I |\mathfrak{g}_I^P(i, j, q) \right. \right. \\ & \left. \left. - \mathcal{G}_2(j, q) - f_{i,j}^\delta(\mathfrak{S}'_i) + \sum_{r=1}^{\mathcal{E}_3(j,q)} \lambda_E |\mathfrak{g}_E^P(i, j, q, r) - \mathcal{G}_3(j, q, r)| \right) \right) \end{aligned} \quad (18a)$$

$$\text{s.t. } \mathfrak{U}_{i,j,q}^2 \leq \mathfrak{U}_{i,b_t,b_t}, \sum_{j,q=1}^{m,\mathcal{E}_2(j)} \mathcal{G}_2(j, q) = 1, \mathfrak{U}_{i,1,1} = 1,$$

$$\mathfrak{U}_i \in \mathbf{S}_+^{6\tilde{p}_2+3m+1} \quad \forall \quad b_t \in \rho^k(j, q, r), t \in [1, 18], i \in [i, n], \\ j \in [1, m], (j, q) \in \mathcal{E}_2, (j, q, r) \in \mathcal{E}_3, \lambda_I > 0, \quad (18b)$$

where \mathfrak{S}'_i is the leading $(m+1) \times (m+1)$ submatrix of \mathfrak{U}_i .

Acceleration with sub-relaxations. Clearly, the matrix \mathfrak{U}_i grows with the number of correspondences m with $\mathcal{O}(m^3)$. Although much faster than standard LMI relaxations, \mathfrak{U}_i slows the SDP solution considerably for p3D. Hence, we base our real-world solution for qE -NRSfM on equation (17) while in section (4) of the supplementary materials, we suggest multiple acceleration strategies for speeding up the SDP solution of equation (18) using edge based relaxation techniques [31] and auxiliary variables, with small sacrifice in reconstruction accuracy.

4. Experimental Results

We describe our experimental results. For our synthetic data experiments, we use a randomised Isometric Surface Generator (ISG) based on [24]. We also propose a technique for extending ISG to Quasi-Equiareal Surface Generator ($qESG$). ISG is associated with a scalar x_σ , the multiplier for additive zero mean Gaussian noise added to the point correspondences. $qESG$ is associated with the scalar χ_E which controls the mean of the uniform random distribution signifying the extent of ‘equiareality’ in the data. The details of ISG, $qESG$ and χ_E are given in section 5 of the supplementary materials. For our real data experiments, we use the following NRSfM benchmarks: *i)* *White Cartoon T-shirt (WC)* and *Hulk* datasets from [7], and *ii)* *Kinect Paper (KP)* dataset from [30]. We also use three dataset containing stretchable objects, obtained from the authors of [5]: *i)* a *Stretched T-shirt (ST)* dataset, *ii)* a *Stretched Leggings (SL)*, and *iii)* a *Squeezed Balloon (SB)*. To validate the capability of our proposed NRSfM techniques to also handle rigid objects, we use the *Model House (MH)* from the VGG

dataset². We compare our methods against [7], [8], [21]-G and [21]-IP (for the general and infinitesimal planarity models resp.), [9], [15], [14] and [12]. We name our solutions from equation (6a)-(6b), (12), (7), (13), (17) and (18) as $sI-\delta$, $sI-P$, $qI-\delta$, $qI-P$, $eI-\delta$, and $eI-P$ (resp.). We use Root Mean Square Error (E_r) and Mean Euclidean Distance (E_d) to quantify the error between reconstruction and Groundtruth (Gt). As with all monocular techniques, our reconstruction is up to scale, which is recovered a posteriori by comparison with Gt . All our solutions are implemented using CVX [13] with MOSEK solver [1] in Matlab.

Strict and quasi-isometric NRSfM. By sharing the same graph structure between \mathcal{E}_2 and NNG for [8] and [15], such that $|\mathcal{E}_2| = kN$, the number of nearest neighbours in NNG, we demonstrate the accuracy of our methods w.r.t increasing $|\mathcal{E}_2|$ in figure 2a. For this, we chose repeated Monte Carlo cross validation by randomly sampling 30% correspondences from ST while varying $|\mathcal{E}_2|$. At low $|\mathcal{E}_2|$ (< 5), our proposed methods $sI-\delta$, $sI-P$, $qI-\delta$ and $qI-P$ are significantly better than [8] and [15], but the gap in accuracy diminishes with increasing neighbours. Figure 2b shows E_r with increasing noise on correspondences. This is done by repeatedly drawing 25% random correspondences from WC and by sharing the same connectivity of $|\mathcal{E}_2| = kN = 7$. All the methods show comparable accuracy within a tolerance, except [15], which is slightly worse. Given simulated data from ISG, we demonstrate the stability of $sI-\delta$, $sI-P$, $qI-\delta$ and $qI-P$ against the closest zeroth-order NRSfM methods [8] and [15] with increasing number of point correspondences in figure 2c. This is done by sharing the same connectivity of $|\mathcal{E}_2| = kN = 5$. All the methods perform comparably but [15] is slightly worse. Our $sI-P$ and $qI-P$ shows slight dip in accuracy with higher correspondences. This is unsurprising, since increasing correspondences without adjusting \mathcal{E}_2 increases the sparsity of $\{\mathfrak{R}_i\}$ and $\{\mathfrak{S}_i\}$ and can be easily compensated back by expanding \mathcal{E}_2 , as evident from figure 2a. To demonstrate the efficacy of our *correspondence completion* method based on equation (14), we repeatedly draw 60% correspondences randomly from KP and log the accuracy for observed and completed missing points by artificially ‘hiding’ up to $\sim 20\%$ correspondence points. This is done with a PN of $s = 3$. The results are shown in figure 2d. The accuracy of correspondence completion remains stable within this range.

We compare our proposed methods with many state-of-the-art methods on hulk, KP, WC and ST datasets in table 1, all values in mm . $qI-P$ is the most accurate method for hulk and KP, while $qI-P$ is 1.59 mm behind [8] in E_r on the WC dataset and LRSB methods [14] and [9] beats $qI-\delta$ by 0.84 and 1.17 mm (resp.) of E_r in ST, which are very small differences in accuracy. Some qualitative plots

are shown in figure (4). Notably, in the highly stretched dataset of ST, all our proposed methods on an average perform 42.8% and 64.9% better than comparable zeroth-order methods [15] and [8], our methods being almost comparable to LRSB in accuracy, while also retaining the same accuracy in the perfectly isometric datasets of WC, KP and hulk, unlike the LRSB methods. We also demonstrate accurate reconstruction of rigid objects with the MH dataset. We create semi-synthetic data by randomly roto-translating the Gt and projecting with arbitrary intrinsics. The results from repeated experiments are given in figure (3), where the strictly isometric methods show accuracies as good as LRSB methods.

Quasi-equiareal NRSfM. We define two error terms: $gE = \frac{1}{n|\mathcal{E}_2|} \sum_{i,j,q=1}^{n,m,\mathcal{E}_2(j)} |\mathcal{G}_2(j,q) - \mathfrak{g}_I(i,j,q)|$ denoting deviation from isometry and $aE = \frac{1}{n|\mathcal{E}_3|} \sum_{i,j,q,r=1}^{n,m,\mathcal{E}_2(j),\mathcal{E}_3(j,q)} |\mathcal{G}_3(j,q,r) - \mathfrak{g}_E(i,j,q,r)|$ denoting deviation from equiareality, where \mathfrak{g}_I and \mathfrak{g}_E are computed geometrically in \mathbb{R}^3 from the unscaled result of $eI-\delta$. In figure 2e, we show an important result: upon repeated experiments on data from $qESG$ with suitable λ_I, λ_E , we manage to control gE independently of aE in $eI-\delta$. Increasing λ_I reduces both gE and aE , as physics mandates. But increasing λ_E forces $eI-\delta$ to find a minimal aE solution without affecting gE . To demonstrate how this affects E_r , we demonstrate synthetic results in figure 2f. Using $qESG$ with increasing equiareality χ_E , we test the E_r for $qI-\delta$, $eI-\delta$, [15] and [8] repeatedly (~ 200 times). Between $qI-\delta$ and $eI-\delta$, λ_I is identical. All four methods share same \mathcal{E}_2 or NNG, \mathcal{E}_3 is derived from the edges of \mathcal{E}_2 . At low χ_E , $qI-\delta$ is better than $eI-\delta$ and similar to [8]. With increasing χ_E , $qI-\delta$ becomes increasingly better than [8] while $eI-\delta$ crosses over at $\chi_E \approx 0.3$ and keeps performing better than $qI-\delta$. Clearly, for equiareal deformations, $qI-\delta$ performs better than [15] and [8] while $eI-\delta$ improves upon this accuracy and remains the most accurate method for all equiareal deformations.

On real data, our experiments on WC, KP, hulk or ST did not yield better results than $qI-\delta$ or $qI-P$, unsurprisingly. Another observation (with details in section 6 of supplementary) is that with denser correspondences, we have smaller simplices and hence isometry dominates over equiareality. Hence, from the data of [5], we select two highly stretchable/squeezable objects SB and SL, and obtain sparse and randomly sampled tracks of 11 correspondences. The results for two such tracks (to be made publicly available with the code) are demonstrated in table 2, compared against all the methods that produced an output, and the accuracy of each frames are shown in figure 2g and 2h. $eI-\delta$ is significantly ahead of all compared methods. Even with denser correspondences, the accuracy from these compared methods do not reach the level of $eI-\delta$. Check section 6 of sup-

²<https://www.robots.ox.ac.uk/~vgg/data/mview>

Table 1. Comparison of $sI-\delta$, $sI-P$, $qI-\delta$ and $qI-P$ with baseline methods

	$sI-\delta$		$sI-P$		$qI-\delta$		$qI-P$		[15]		[8]		[21]-IP		[21]-G		[14]		[12]		[9]		[7]	
	E_r	E_d	E_r	E_d	E_r	E_d	E_r	E_d	E_r	E_d	E_r	E_d	E_r	E_d	E_r	E_d	E_r	E_d	E_r	E_d	E_r	E_d	E_r	E_d
Hulk	2.49	1.94	2.19	1.68	2.53	1.98	2.19	1.68	2.58	2.10	2.53	1.87	11.10	9.64	11.25	9.81	19.34	18.33	34.61	32.18	16.59	15.00	16.72	14.93
KP	4.76	4.17	3.93	3.53	4.53	3.98	3.85	3.47	9.06	7.57	4.77	4.25	11.30	10.12	11.34	10.14	13.25	11.87	30.61	28.40	13.40	12.12	13.88	12.12
WC	9.39	7.54	7.45	5.97	8.78	7.11	7.39	5.92	5.8	4.57	9.72	7.88	21.45	18.69	21.54	18.79	66.28	62.78	106.89	95.24	25.7	22.91	26.54	23.38
ST	8.65	6.79	8.64	6.68	8.53	6.71	8.61	6.66	24.54	20.71	15.05	12.39	11.97	10.85	11.82	10.72	7.69	7.14	13.41	12.01	7.36	6.79	9.30	8.69

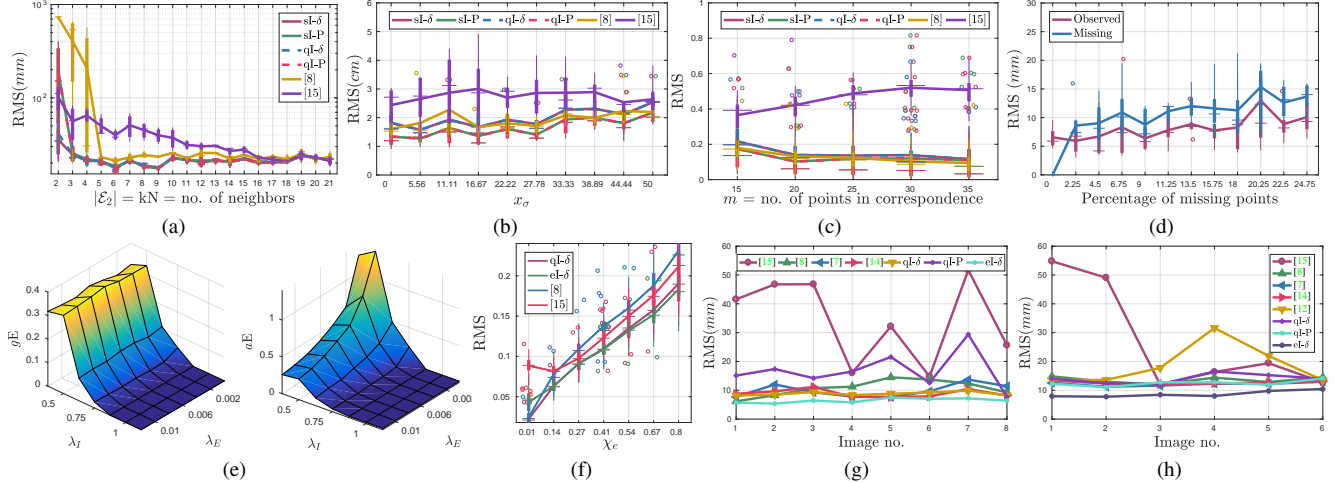


Figure 2. We show the following: (a) the variation of E_r w.r.t increasing neighbors in \mathcal{E}_2 , (b) the variation of E_r w.r.t additive pixel noise to correspondences, (c) the variation of E_r , in Arbitrary Units (au), w.r.t increasing m for same \mathcal{E}_2 (or NNG) for all compared methods, (d) the variation of E_r in observed and missing correspondences completed by $qI-P$, (e) the variation of gE and aE w.r.t changes in λ_I and λ_E , (f) the variation of E_r in au w.r.t increasing χ_E in $qESG$, (g) and (h) E_r for each frame from SL and SB respectively.

 Table 2. $qI-\delta$, $qI-P$ and $eI-\delta$ against baseline methods (in mm)

		[15]	[8]	[12]	[14]	[7]	$qI-\delta$	$qI-P$	$eI-\delta$
SB	E_r	27.36	13.59	18.66	12.66	12.11	13.53	12.48	8.72
	E_d	21.07	11.47	17.63	11.36	10.95	10.09	9.92	7.19
SL	E_r	34.43	10.78	x	8.92	10.41	8.81	8.67	6.43
	E_d	31.53	8.65	x	8.00	9.36	7.70	7.55	5.59

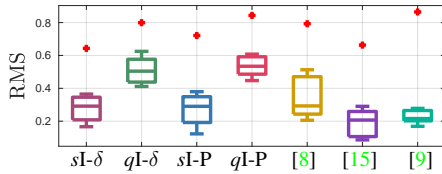
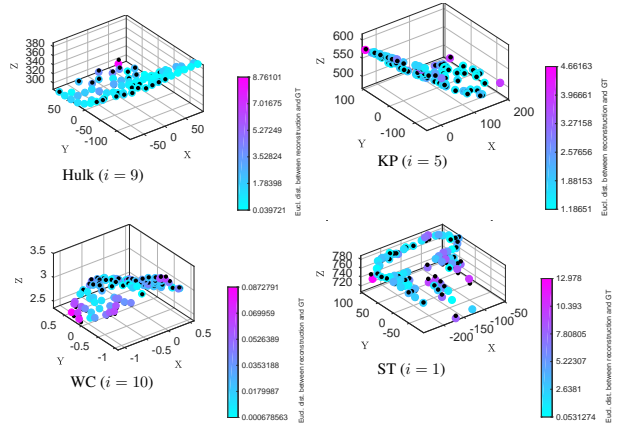


Figure 3. Results from MH rigid dataset.

plementary for validation across varying resolutions for SB and SL, as well as extended analysis of all our experiments.

5. Conclusion

We have presented a convex formulation for strict and quasi-isometric NRSfM, as well as extended the method to handle quasi-equiareality. Our solution for sI -NRSfM and qI -NRSfM solves the restrictive isometry problem without utilising inextensible relaxations, which is a first for ze-


 Figure 4. Qualitative results from $sI-P$. Black points are G_t .

roth order NRSfM methods. Our solution for qE -NRSfM presents the first method handling quasi-equiareality convexly, searching for nearly equiareal solution in the vicinity of the solution space of quasi-isometry. We demonstrate that sI -NRSfM and qI -NRSfM achieve state-of-the-art accuracy in benchmark datasets and are more generalisable to extensible surfaces than comparable methods. We demonstrate that for highly extensible surfaces, our solution to qE -NRSfM produces reconstruction of unmatched accuracy.

Acknowledgement

We thank the authors of [5] for helping us out by sharing and explaining their dataset to us. This project has received funding from the European Union’s Horizon 2020 research and innovation programme under grant agreement No 863146.

References

- [1] MOSEK ApS. *The MOSEK optimization toolbox for MATLAB manual. Version 9.0.*, 2019. 7
- [2] Maria Belk. Realizability of graphs in three dimensions. *Discrete & Computational Geometry*, 37(2):139–162, 2007. 2
- [3] Pratik Biswas, Kim-Chuan Toh, and Yinyu Ye. A distributed sdp approach for large-scale noisy anchor-free graph realization with applications to molecular conformation. *SIAM Journal on Scientific Computing*, 30(3):1251–1277, 2008. 2
- [4] Emmanuel J Candès and Terence Tao. The power of convex relaxation: Near-optimal matrix completion. *IEEE Transactions on Information Theory*, 56(5):2053–2080, 2010. 2
- [5] David Casillas-Perez, Daniel Pizarro, David Fuentes-Jimenez, Manuel Mazo, and Adrien Bartoli. Equiareal shape-from-template. *Journal of Mathematical Imaging and Vision*, 61(5):607–626, 2019. 2, 6, 7, 9
- [6] Yongbo Chen, Liang Zhao, Yanhao Zhang, and Shoudong Huang. Dense isometric non-rigid shape-from-motion based on graph optimization and edge selection. *IEEE Robotics and Automation Letters*, 5(4):5889–5896, 2020. 1, 2
- [7] Ajad Chhatkuli, Daniel Pizarro, and Adrien Bartoli. Non-rigid shape-from-motion for isometric surfaces using infinitesimal planarity. In *BMVC*, 2014. 1, 2, 6, 7, 8
- [8] Ajad Chhatkuli, Daniel Pizarro, Toby Collins, and Adrien Bartoli. Inextensible non-rigid structure-from-motion by second-order cone programming. *IEEE transactions on pattern analysis and machine intelligence*, 40(10):2428–2441, 2017. 1, 2, 7, 8
- [9] Yuchao Dai, Hongdong Li, and Mingyi He. A simple prior-free method for non-rigid structure-from-motion factorization. *International Journal of Computer Vision*, 107(2):101–122, 2014. 1, 7, 8
- [10] Manfredo P Do Carmo. *Differential geometry of curves and surfaces: revised and updated second edition*. Courier Dover Publications, 2016. 2
- [11] Michael S Floater and Kai Hormann. Surface Parameterization: a Tutorial and Survey. In Neil A Dodgson, Michael S Floater, and Malcolm A Sabin, editors, *Advances in Multiresolution for Geometric Modelling*, pages 157–186, Berlin, Heidelberg, 2005. Springer Berlin Heidelberg. 1, 2
- [12] Paulo FU Gotardo and Aleix M Martinez. Kernel non-rigid structure from motion. In *2011 International Conference on Computer Vision*, pages 802–809. IEEE, 2011. 1, 7, 8
- [13] M. Grant and S. Boyd. Graph implementations for nonsmooth convex programs. In V. Blondel, S. Boyd, and H. Kimura, editors, *Recent Advances in Learning and Control*, Lecture Notes in Control and Information Sciences, pages 95–110. Springer-Verlag Limited, 2008. http://stanford.edu/~boyd/graph_dcp.html. 7
- [14] Onur C Hamsici, Paulo FU Gotardo, and Aleix M Martinez. Learning spatially-smooth mappings in non-rigid structure from motion. In *European Conference on computer vision*, pages 260–273. Springer, 2012. 7, 8
- [15] Pan Ji, Hongdong Li, Yuchao Dai, and Ian Reid. "maximizing rigidity" revisited: a convex programming approach for generic 3d shape reconstruction from multiple perspective views. In *Proceedings of the IEEE International Conference on Computer Vision*, pages 929–937, 2017. 1, 2, 7, 8
- [16] Gangshan Jing, Changhuang Wan, and Ran Dai. Angle-based sensor network localization. *IEEE Transactions on Automatic Control*, 67(2):840–855, 2021. 3
- [17] Suryansh Kumar. Non-rigid structure from motion: Prior-free factorization method revisited. In *Proceedings of the IEEE/CVF Winter Conference on Applications of Computer Vision*, pages 51–60, 2020. 1
- [18] Suryansh Kumar and Luc Van Gool. Organic priors in non-rigid structure from motion. *arXiv preprint arXiv:2207.06262*, 2022. 1
- [19] Jean B Lasserre. Convergent lmi relaxations for nonconvex quadratic programs. In *Proceedings of the 39th IEEE Conference on Decision and Control (Cat. No. 00CH37187)*, volume 5, pages 5041–5046. IEEE, 2000. 4, 5
- [20] Jean B Lasserre. Convergent sdp-relaxations in polynomial optimization with sparsity. *SIAM Journal on Optimization*, 17(3):822–843, 2006. 2
- [21] Shaifali Parashar, Daniel Pizarro, and Adrien Bartoli. Isometric non-rigid shape-from-motion with riemannian geometry solved in linear time. *IEEE transactions on pattern analysis and machine intelligence*, 40(10):2442–2454, 2017. 1, 2, 7, 8
- [22] Shaifali Parashar, Daniel Pizarro, and Adrien Bartoli. Local deformable 3d reconstruction with cartan’s connections. *IEEE transactions on pattern analysis and machine intelligence*, 42(12):3011–3026, 2019. 1, 2
- [23] Shaifali Parashar, Mathieu Salzmann, and Pascal Fua. Local non-rigid structure-from-motion from diffeomorphic mappings. In *Proceedings of the IEEE/CVF Conference on Computer Vision and Pattern Recognition*, pages 2059–2067, 2020. 1, 2
- [24] Mathieu Perriollat and Adrien Bartoli. A computational model of bounded developable surfaces with application to image-based three-dimensional reconstruction. *Computer Animation and Virtual Worlds*, 24(5):459–476, 2013. 6
- [25] Mathieu Perriollat, Richard Hartley, and Adrien Bartoli. Monocular template-based reconstruction of inextensible surfaces. *International journal of computer vision*, 95(2):124–137, 2011. 2
- [26] Thomas Probst, Danda Pani Paudel, Ajad Chhatkuli, and Luc Van Gool. Convex relaxations for consensus and non-minimal problems in 3d vision. In *Proceedings of the IEEE/CVF International Conference on Computer Vision*, pages 10233–10242, 2019. 3
- [27] Thomas Probst, Danda Pani Paudel, Ajad Chhatkuli, and Luc Van Gool. Incremental non-rigid structure-from-motion with unknown focal length. In *Proceedings of the European Conference on Computer Vision (ECCV)*, pages 756–771, 2018. 1

- [28] Mathieu Salzmann and Pascal Fua. Linear local models for monocular reconstruction of deformable surfaces. *IEEE Transactions on Pattern Analysis and Machine Intelligence*, 33(5):931–944, 2010. 2
- [29] Anthony Man-Cho So and Yinyu Ye. Theory of semidefinite programming for sensor network localization. *Mathematical Programming*, 109(2):367–384, 2007. 2
- [30] Aydin Varol, Mathieu Salzmann, Pascal Fua, and Raquel Urtasun. A constrained latent variable model. In *2012 IEEE conference on computer vision and pattern recognition*, pages 2248–2255. Ieee, 2012. 6
- [31] Zizhuo Wang, Song Zheng, Yinyu Ye, and Stephen Boyd. Further relaxations of the semidefinite programming approach to sensor network localization. *SIAM Journal on Optimization*, 19(2):655–673, 2008. 6

Supplementary Materials

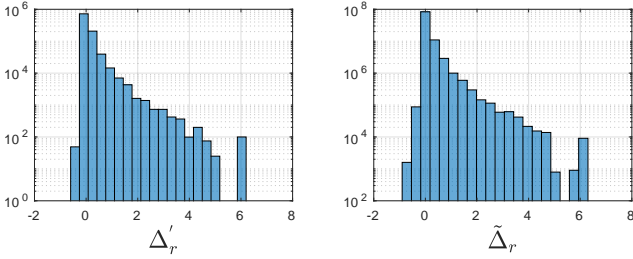


Figure 1. *left*: the discriminant Δ'_r of the solution for $\delta'_{i,r}$ from equation (2), sampled over 1 million times with randomly drawn 3D vertices forming a triangle with $h_1 \in [0, 0.1]$, *right*: the discriminant $\tilde{\Delta}_r$ of the solution for $\tilde{\delta}_{i,r}$ from equation (3), sampled over 1 million times with similarly drawn 3D vertices with $(h_1, h_2) \in [0, 0.1]$, where the average edge length of all the triangles is ~ 0.6 units. $(\Delta'_r, \tilde{\Delta}_r)$ are positive, ensuring real solution, for a clear majority of cases

We describe additional details of our article in this supplementary material. To recap, we had provided convex solutions to isometric and quasi-isometric NRSfM in the main article, as well as a convex solution for quasi-equiareal NRSfM. Table (1) summarizes the position of our contributions w.r.t existing NRSfM state-of-the-art.

Following up from our main article, we provide the following: section (1) provides the proof of Lemma 1, section (2) provides the details of the quartics involved in area computation, section (3) provides details of how to express these quartics as linear combination of elements of the Gram matrices $\{\mathcal{T}_i\}$ and $\{\mathcal{U}_i\}$, section (4) provides strategies for accelerating the p 3D solution for q E-NRSfM, section (5) details the methodology for generating the synthetic data used in our experiments, and section (6) provides additional experimental results, both qualitative and quantitative.

1. Proof of Lemma 1

A 2-simplex with vertices lying strictly on three non-degenerate SLs with an additional equiareality constraint has 2 degrees of freedom. Therefore, with 3 independent variables (using DaSL for the simplest parameterisation), we have the following minimal case: 4 vertices forming a fully connected graph, i.e., $|\mathcal{E}_2| = 5$ and $|\mathcal{E}_3| = 3$ observed

across 3 images gives us 12 equations for 12 variables, hence *solvable* in theory. However, lemma 1 posits that such a solution, if it exists, is non-unique for the NRSfM problem.

The squared area of a 2-simplex enclosed by $(\mathbf{P}_{i,j}, \mathbf{P}_{i,q}, \mathbf{P}_{i,r})$ is given by the element-wise expansion of the vector product of any two edges of the triangle formed by those three vertices, given by:

$$\begin{aligned} \mathfrak{h}_E^\delta(i, j, q, r) &= \left(\text{Area}(\mathbf{P}_{i,j}, \mathbf{P}_{i,q}, \mathbf{P}_{i,r}) \right)^2 = \\ &= \left(\frac{1}{2} \| (\delta_{i,j} \mathbf{d}_{i,j} - \delta_{i,q} \mathbf{d}_{i,q}) \times (\delta_{i,r} \mathbf{d}_{i,r} - \delta_{i,q} \mathbf{d}_{i,q}) \| \right)^2 \\ &= \frac{1}{4} \left(\left(G_1^{i,j,q,r} \delta_{i,q}^2 + G_2^{i,j,q,r} \delta_{i,r} \delta_{i,q} + G_3^{i,j,q,r} \delta_{i,r}^2 \right) \delta_{i,j}^2 + \right. \\ &\quad \left. \left(G_4^{i,j,q,r} \delta_{i,r} \delta_{i,q}^2 + G_5^{i,j,q,r} \delta_{i,r}^2 \delta_{i,q} \right) \delta_{i,j} + G_6^{i,j,q,r} \delta_{i,q}^2 \delta_{i,r}^2 \right), \end{aligned} \quad (1)$$

where $G_1^{i,j,q,r}, \dots, G_6^{i,j,q,r}$ are data-terms derived from the SLs (check section 2 for details).

The proof of lemma 1 follows.

Proof. Given the triangle enclosed by $(\mathbf{P}_{i,j}, \mathbf{P}_{i,q}, \mathbf{P}_{i,r})$, we claim the following:

Ansatz 1: for some small displacement h_1 applied to $\delta_{i,j}$, there exists a corrective displacement $\delta'_{i,r}$ such that the triangles at depth $(\delta_{i,j}, \delta_{i,q}, \delta_{i,r})$ and $(\delta_{i,j} + h_1, \delta_{i,q}, \delta'_{i,r})$ of SLs $(\mathbf{d}_{i,j}, \mathbf{d}_{i,q}, \mathbf{d}_{i,r})$ have the same area. We prove this by equating the squared area of the two triangles, giving us:

$$\begin{aligned} &\left(\left(G_1^{i,j,q,r} \delta_{i,q}^2 + G_2^{i,j,q,r} \delta_{i,r} \delta_{i,q} + G_3^{i,j,q,r} \delta_{i,r}^2 \right) \delta_{i,j}^2 + \right. \\ &\quad \left. \left(G_4^{i,j,q,r} \delta_{i,r} \delta_{i,q}^2 + G_5^{i,j,q,r} \delta_{i,r}^2 \delta_{i,q} \right) \delta_{i,j} + G_6^{i,j,q,r} \delta_{i,q}^2 \delta_{i,r}^2 \right) = \\ &\quad \left(\left(G_1^{i,j,q,r} \delta_{i,q}^2 + G_2^{i,j,q,r} \delta'_{i,r} \delta_{i,q} + G_3^{i,j,q,r} (\delta'_{i,r})^2 \right) (\delta_{i,j} + h_1)^2 \right. \\ &\quad \left. + \left(G_4^{i,j,q,r} \delta'_{i,r} \delta_{i,q}^2 + G_5^{i,j,q,r} (\delta'_{i,r})^2 \delta_{i,q} \right) (\delta_{i,j} + h_1) \right. \\ &\quad \left. + G_6^{i,j,q,r} \delta_{i,q}^2 (\delta'_{i,r})^2 \right) \end{aligned} \quad (2)$$

	Problem formulation	Assumptions	Existing convex methods
Isometric NRSfM	$\min \quad 0,$ $\text{s.t.: } \mathbf{g}_I(i, j, q) = \mathcal{G}_2(j, q)$ $\forall i \in [1, n], j \in [1, m], (j, q) \in \mathcal{E}_2$	Euclidean distances approximate geodesic distances	-
Isometric NRSfM with MDH	$\min \quad - \sum_{1,j=1}^{n,m} \delta_{i,j},$ $\text{s.t.: } \mathbf{g}_I(i, j, q) = \mathcal{G}_2(j, q)$ $\forall i \in [1, n], j \in [1, m], (j, q) \in \mathcal{E}_2$	Euclidean distances approximate geodesic distances, MDH	-
Inextendible NRSfM with MDH	$\min \quad - \sum_{1,j=1}^{n,m} \delta_{i,j},$ $\text{s.t.: } \mathbf{g}_I(i, j, q) \leq \mathcal{G}_2(j, q)$ $\forall i \in [1, n], j \in [1, m], (j, q) \in \mathcal{E}_2$	Euclidean distances approximate geodesic distances, MDH, inextendibility	[3] [8]

Table 1. Hierarchy of isometric NRSfM problems. The solutions we provide to sI-NRSfM and qI-NRSfM are reformulations of ‘isometric NRSfM with MDH’, while purely ‘isometric NRSfM’ is uninteresting, since it does not have an unique solution

Solving for $\delta'_{i,r}$ leads to a hexic discriminant¹. Hence existence of a real solution cannot be ensured analytically. However, we show with extensive exhaustive randomized simulations that for all small values of h_1 , a real $\delta'_{i,r}$ is obtainable in most cases. Check figure 1 for details.

Ansatz 2: there exist small displacements h_1 and h_2 which, when applied to $\delta_{i,j}$ and $\delta_{i,q}$, can change the area of the triangle in $(\mathbf{P}_{i,j}, \mathbf{P}_{i,q}, \mathbf{P}_{i,r})$ but can be exactly compensated by a corrective displacement $\tilde{\delta}_{i,r}$. This is derived by similarly equating the two squared areas:

$$\begin{aligned}
& \left(\left(G_1^{i,j,q,r} \delta_{i,q}^2 + G_2^{i,j,q,r} \delta_{i,r} \delta_{i,q} + G_3^{i,j,q,r} \delta_{i,r}^2 \right) \delta_{i,j}^2 + \right. \\
& \left. \left(G_4^{i,j,q,r} \delta_{i,r} \delta_{i,q}^2 + G_5^{i,j,q,r} \delta_{i,r}^2 \delta_{i,q} \right) \delta_{i,j} + G_6^{i,j,q,r} \delta_{i,q}^2 \delta_{i,r}^2 \right) = \\
& \left(\left(G_1^{i,j,q,r} (\delta_{i,q} + h_2)^2 + G_2^{i,j,q,r} \tilde{\delta}_{i,r} (\delta_{i,q} + h_2) + G_3^{i,j,q,r} \tilde{\delta}_{i,r}^2 \right) \right. \\
& \left. (\delta_{i,j} + h_1)^2 + \left(G_4^{i,j,q,r} \tilde{\delta}_{i,r} (\delta_{i,q} + h_2)^2 + G_5^{i,j,q,r} \tilde{\delta}_{i,r}^2 \right) \right. \\
& \left. (\delta_{i,q} + h_2) \right) (\delta_{i,j} + h_1) + G_6^{i,j,q,r} (\delta_{i,q} + h_2)^2 \tilde{\delta}_{i,r}^2 \quad (3)
\end{aligned}$$

Solving for $\tilde{\delta}_{i,r}$ leads to another solution with a hexic discriminant. Again using randomized simulations, we show that there exist many combinations of (h_1, h_2) with $(\mathbf{P}_{i,j}, \mathbf{P}_{i,q}, \mathbf{P}_{i,r})$ which leads to a real solution for $\tilde{\delta}_{i,r}$. as shown in figure (1).

Combining *ansatz 1* with *ansatz 2*, we can say the following: given vertices $\mathbf{P}_{i,1}, \dots, \mathbf{P}_{i,m}$, there can exist a lo-

¹Maple scripts for generating the full solution of $\delta'_{i,r}$ (and $\tilde{\delta}_{i,r}$ later) has been provided with the supplementary

cally acyclic graph structure on these vertices such that the change of area due to arbitrary displacement of one of the vertices can be compensated by some other displacement of some other vertices. Hence, the vertices are non-unique. Given that in NRSfM the areas are also unknown, not just the depth of the points, this makes purely equiareal NRSfM highly ambiguous. \square

Such a proof precludes the possibility of defining specially constrained graph structures (e.g.: locally cyclic Whitney triangulation etc.) on the vertices to enforce unique solution, but such graph structures are unavailable for NRSfM, hence not considered.

2. Quartics for Area Computation

We now describe the details of h_E^δ and h_E^P , the squared area of 2-simplices in DaSL and p3D respectively. Beginning with h_E^δ , which can be expressed by equation (1), where:

$$\begin{aligned}
G_1^{i,j,q,r} = & (y_{i,q}^2 + z_{i,q}^2)x_{i,j}^2 - 2(y_{i,q}x_{i,q}y_{i,j} + z_{i,q}x_{i,q}z_{i,j})x_{i,j} \\
& + (z_{i,q}^2 + x_{i,q}^2)y_{i,j}^2 - 2z_{i,q}y_{i,q}z_{i,j}y_{i,j} + (y_{i,q}^2 + x_{i,q}^2)z_{i,j}^2, \quad (4a)
\end{aligned}$$

$$\begin{aligned}
G_2^{i,j,q,r} = & -2(y_{i,q}y_{i,r} + z_{i,r}z_{i,q})x_{i,j}^2 - 2((-x_{i,r}y_{i,q} \\
& - x_{i,q}y_{i,r})y_{i,j} + (-x_{i,r}z_{i,q} - z_{i,r}x_{i,q})z_{i,j})x_{i,j} - 2(z_{i,r}z_{i,q} \\
& + x_{i,q}x_{i,r})y_{i,j}^2 + 2(z_{i,r}y_{i,q} + z_{i,q}y_{i,r})z_{i,j}y_{i,j} \\
& - 2(y_{i,q}y_{i,r} + x_{i,q}x_{i,r})z_{i,j}^2, \quad (4b)
\end{aligned}$$

$$G_3^{i,j,q,r} = (y_{i,r}^2 + z_{i,r}^2)x_{i,j}^2 - 2(y_{i,r}x_{i,r}y_{i,j} + z_{i,r}x_{i,r}z_{i,j})x_{i,j}$$

$$+(x_{i,r}^2 + z_{i,r}^2)y_{i,j}^2 - 2y_{i,j}z_{i,j}y_{i,r}z_{i,r} + z_{i,j}^2(x_{i,r}^2 + y_{i,r}^2), \quad (4c)$$

$$G_4^{i,j,q,r} = 2 \left((y_{i,q}y_{i,r} + z_{i,r}z_{i,q})x_{i,q} - x_{i,r}(y_{i,q}^2 + (z_{i,q})^2)x_{i,j} - 2(-z_{i,r}z_{i,q}y_{i,q} - x_{i,r}y_{i,q}x_{i,q} + z_{i,q}^2y_{i,r} + x_{i,q}^2y_{i,r})y_{i,j} - 2(y_{i,q}^2z_{i,r} - z_{i,q}y_{i,r}y_{i,q} - x_{i,r}z_{i,q}x_{i,q} + x_{i,q}^2z_{i,r})z_{i,j}, \right. \quad (4d)$$

$$G_5^{i,j,q,r} = 2 \left(-(y_{i,r}^2 + z_{i,r}^2)x_{i,q} - x_{i,r}(-y_{i,q}y_{i,r} - z_{i,r}z_{i,q})x_{i,j} - 2(-x_{i,r}y_{i,r}x_{i,q} + (x_{i,r}^2 + z_{i,r}^2)y_{i,q} - z_{i,q}y_{i,r}z_{i,r})y_{i,j} - 2(-x_{i,r}z_{i,r}x_{i,q} - y_{i,r}z_{i,r}y_{i,q} + z_{i,q}(x_{i,r}^2 + y_{i,r}^2))z_{i,j}, \right. \quad (4e)$$

$$G_6^{i,j,q,r} = (y_{i,r}^2 + z_{i,r}^2)x_{i,q}^2 - 2x_{i,r}(y_{i,q}y_{i,r} + z_{i,r}z_{i,q})x_{i,q} + (x_{i,r}^2 + z_{i,r}^2)y_{i,q}^2 - 2z_{i,q}y_{i,r}z_{i,r}y_{i,q} + z_{i,q}^2(x_{i,r}^2 + y_{i,r}^2). \quad (4f)$$

Similarly expanding for h_E^P , we have:

$$\begin{aligned} h_E^P(i, j, q, r) &= \left(\text{Area}(\mathbf{P}_{i,j}, \mathbf{P}_{i,q}, \mathbf{P}_{i,r}) \right)^2 \\ &= \frac{1}{4} \left(X_{i,j}^2 Y_{i,q}^2 - 2X_{i,j}^2 Y_{i,q} Y_{i,r} + X_{i,j}^2 Y_{i,r}^2 + X_{i,j}^2 Z_{i,q}^2 \right. \\ &\quad - 2X_{i,j}^2 Z_{i,q} Z_{i,r} + X_{i,j}^2 Z_{i,r}^2 - 2X_{i,j} X_{i,q} Y_{i,j} Y_{i,q} \\ &\quad + 2X_{i,j} X_{i,q} Y_{i,j} Y_{i,r} + 2X_{i,j} X_{i,q} Y_{i,q} Y_{i,r} - 2X_{i,j} X_{i,q} Y_{i,r}^2 - \\ &\quad 2X_{i,j} X_{i,q} Z_{i,j} Z_{i,q} + 2X_{i,j} X_{i,q} Z_{i,j} Z_{i,r} + 2X_{i,j} X_{i,q} Z_{i,q} Z_{i,r} \\ &\quad - 2X_{i,j} X_{i,q} Z_{i,r}^2 + 2X_{i,j} X_{i,r} Y_{i,j} Y_{i,q} - 2X_{i,j} X_{i,r} Y_{i,j} Y_{i,r} \\ &\quad - 2X_{i,j} X_{i,r} Y_{i,q}^2 + 2X_{i,j} X_{i,r} Y_{i,q} Y_{i,r} + 2X_{i,j} X_{i,r} Z_{i,j} Z_{i,q} \\ &\quad - 2X_{i,j} X_{i,r} Z_{i,j} Z_{i,r} - 2X_{i,j} X_{i,r} Z_{i,q}^2 + 2X_{i,j} X_{i,r} Z_{i,q} Z_{i,r} \\ &\quad + X_{i,q}^2 Y_{i,j}^2 - 2X_{i,q}^2 Y_{i,j} Y_{i,r} + X_{i,q}^2 Y_{i,r}^2 \\ &\quad + X_{i,q}^2 Z_{i,j}^2 - 2X_{i,q}^2 Z_{i,j} Z_{i,r} + X_{i,q}^2 Z_{i,r}^2 \\ &\quad - 2X_{i,q} X_{i,r} Y_{i,j}^2 + 2X_{i,q} X_{i,r} Y_{i,j} Y_{i,q} + 2X_{i,q} X_{i,r} Y_{i,j} Y_{i,r} \\ &\quad - 2X_{i,q} X_{i,r} Y_{i,q} Y_{i,r} - 2X_{i,q} X_{i,r} Z_{i,j}^2 + 2X_{i,q} X_{i,r} Z_{i,j} Z_{i,q} + \\ &\quad 2X_{i,q} X_{i,r} Z_{i,j} Z_{i,r} - 2X_{i,q} X_{i,r} Z_{i,q} Z_{i,r} + X_{i,r}^2 Y_{i,j}^2 \\ &\quad - 2X_{i,r}^2 Y_{i,j} Y_{i,q} + X_{i,r}^2 Y_{i,q}^2 + X_{i,r}^2 Z_{i,j}^2 \\ &\quad - 2X_{i,r}^2 Z_{i,j} Z_{i,q} + X_{i,r}^2 Z_{i,q}^2 + Y_{i,j}^2 Z_{i,q}^2 \\ &\quad - 2Y_{i,j}^2 Z_{i,q} Z_{i,r} + Y_{i,j}^2 Z_{i,r}^2 - 2Y_{i,j} Y_{i,q} Z_{i,j} Z_{i,q} \\ &\quad + 2Y_{i,j} Y_{i,q} Z_{i,j} Z_{i,r} + 2Y_{i,j} Y_{i,q} Z_{i,q} Z_{i,r} - 2Y_{i,j} Y_{i,q} Z_{i,r}^2 \\ &\quad + 2Y_{i,j} Y_{i,r} Z_{i,j} Z_{i,q} - 2Y_{i,j} Y_{i,r} Z_{i,j} Z_{i,r} - 2Y_{i,j} Y_{i,r} Z_{i,q}^2 \\ &\quad + 2Y_{i,j} Y_{i,r} Z_{i,q} Z_{i,r} + Y_{i,q}^2 Z_{i,j}^2 - 2Y_{i,q}^2 Z_{i,j} Z_{i,r} \\ &\quad + Y_{i,q}^2 Z_{i,r}^2 - 2Y_{i,q} Y_{i,r} Z_{i,j}^2 + 2Y_{i,q} Y_{i,r} Z_{i,j} Z_{i,q} \\ &\quad + 2Y_{i,q} Y_{i,r} Z_{i,j} Z_{i,r} - 2Y_{i,q} Y_{i,r} Z_{i,q} Z_{i,r} + Y_{i,r}^2 Z_{i,j}^2 \\ &\quad \left. - 2Y_{i,r}^2 Z_{i,j} Z_{i,q} + Y_{i,r}^2 Z_{i,q}^2 \right). \quad (5) \end{aligned}$$

3. Area from Gram Matrices

We now describe the functions g_E^δ and g_E^P that compute squared area from linear combination of the elements of \mathfrak{T}_i and \mathfrak{U}_i respectively. Beginning with g_E^δ :

$$g_E^\delta(i, j, q, r) = \frac{1}{4} (G_1^{i,j,q,r}, \dots, G_6^{i,j,q,r})^\top \begin{pmatrix} \mathfrak{T}_{i,a_1,a_1} \\ \mathfrak{T}_{i,a_1,c_1} \\ \mathfrak{T}_{i,c_1,c_1} \\ \mathfrak{T}_{i,a_1,b_1} \\ \mathfrak{T}_{i,b_1,c_1} \\ \mathfrak{T}_{i,b_1,b_1} \end{pmatrix}, \quad (6)$$

where $\mathfrak{E}_{i,a_1} = \delta_{i,j}\delta_{i,q}$, $\mathfrak{E}_{i,b_1} = \delta_{i,q}\delta_{i,r}$ and, $\mathfrak{E}_{i,c_1} = \delta_{i,j}\delta_{i,r}$.

Next, we describe g_E^P as a linear combination of elements of \mathfrak{U}_i . Deriving from equation (5):

$$\begin{aligned} g_E^P(i, j, q, r) &= \frac{1}{4} \left(\mathfrak{U}_{i,d_1,d_1} - 2\mathfrak{U}_{i,d_1,f_1} + \mathfrak{U}_{i,f_1,f_1} + \mathfrak{U}_{i,e_1,e_1} \right. \\ &\quad - 2\mathfrak{U}_{i,e_1,g_1} + \mathfrak{U}_{i,g_1,g_1} - 2\mathfrak{U}_{i,d_1,h_1} + 2\mathfrak{U}_{i,f_1,h_1} \\ &\quad + 2\mathfrak{U}_{i,d_1,p_1} - 2\mathfrak{U}_{i,f_1,p_1} - 2\mathfrak{U}_{i,e_1,l_1} + 2\mathfrak{U}_{i,g_1,l_1} \\ &\quad + 2\mathfrak{U}_{i,e_1,q_1} - 2\mathfrak{U}_{i,g_1,q_1} + 2\mathfrak{U}_{i,d_1,j_1} - 2\mathfrak{U}_{i,f_1,j_1} - \\ &\quad 2\mathfrak{U}_{i,d_1,r_1} + 2\mathfrak{U}_{i,f_1,r_1} + 2\mathfrak{U}_{i,e_1,n_1} - 2\mathfrak{U}_{i,g_1,n_1} \\ &\quad - 2\mathfrak{U}_{i,e_1,t_1} + 2\mathfrak{U}_{i,g_1,t_1} + \mathfrak{U}_{i,h_1,h_1} - 2\mathfrak{U}_{i,h_1,p_1} \\ &\quad + \mathfrak{U}_{i,p_1,p_1} + \mathfrak{U}_{i,l_1,l_1} - 2\mathfrak{U}_{i,l_1,q_1} + \mathfrak{U}_{i,q_1,q_1} - 2\mathfrak{U}_{i,h_1,j_1} \\ &\quad + 2\mathfrak{U}_{i,h_1,r_1} + 2\mathfrak{U}_{i,j_1,p_1} - 2\mathfrak{U}_{i,p_1,r_1} - 2\mathfrak{U}_{i,l_1,n_1} \\ &\quad + 2\mathfrak{U}_{i,l_1,t_1} + 2\mathfrak{U}_{i,n_1,q_1} - 2\mathfrak{U}_{i,q_1,t_1} + \mathfrak{U}_{i,j_1,j_1} - \\ &\quad 2\mathfrak{U}_{i,j_1,r_1} + \mathfrak{U}_{i,r_1,r_1} + \mathfrak{U}_{i,n_1,n_1} - 2\mathfrak{U}_{i,n_1,t_1} + \mathfrak{U}_{i,t_1,t_1} \\ &\quad + \mathfrak{U}_{i,i_1,i_1} - 2\mathfrak{U}_{i,i_1,k_1} + \mathfrak{U}_{i,k_1,k_1} - 2\mathfrak{U}_{i,i_1,m_1} + 2\mathfrak{U}_{i,k_1,m_1} \\ &\quad + 2\mathfrak{U}_{i,i_1,s_1} - 2\mathfrak{U}_{i,k_1,s_1} + 2\mathfrak{U}_{i,i_1,o_1} - 2\mathfrak{U}_{i,k_1,o_1} - \\ &\quad 2\mathfrak{U}_{i,i_1,u_1} + 2\mathfrak{U}_{i,k_1,u_1} + \mathfrak{U}_{i,m_1,m_1} - 2\mathfrak{U}_{i,m_1,s_1} \\ &\quad + \mathfrak{U}_{i,s_1,s_1} - 2\mathfrak{U}_{i,m_1,o_1} + 2\mathfrak{U}_{i,m_1,u_1} + 2\mathfrak{U}_{i,o_1,s_1} \\ &\quad \left. - 2\mathfrak{U}_{i,s_1,u_1} + \mathfrak{U}_{i,o_1,o_1} - 2\mathfrak{U}_{i,o_1,u_1} + \mathfrak{U}_{i,u_1,u_1} \right), \quad (7) \end{aligned}$$

where $\mathfrak{Q}_{i,d_1} = X_{i,j}Y_{i,q}$, $\mathfrak{Q}_{i,f_1} = X_{i,j}Y_{i,r}$, and so on. Clearly, (d_1, \dots, u_1) is exactly mappable from the definition of \mathfrak{Q}_i in equation (15) of the main paper using the map $\vartheta(i, j, q)$.

4. Accelerating p3D Solution for qE-NRSfM

We now present a method for accelerating the qE-NRSfM solution in equation (18) of the main paper.

Edge based relaxation. If \mathcal{E}_3 does not represent all 2-simplices from a fully connected graph in the vertices of \mathbf{X}_i , $\{\mathfrak{U}_i\}$ is a partial PSD matrix with a sparsely connected structure and standard SDP solvers do not guarantee a rank-1 PSD completion of $\{\mathfrak{U}_i\}$ while solving equations (18) [11]. However, for our NRSfM problem, an edge

in \mathcal{E}_2 cannot be connected beyond its local neighborhood, hence an exact rank-1 completion of $\{\mathcal{U}_i\}$ is not mandatory. However, there exist principal submatrices of $\{\mathcal{U}_i\}$ (in \mathbf{S}_+^{18}) corresponding to the connected 2-simplices for which an exact rank-1 completion is desirable. Therefore we can relax the PSD constraint on the full matrices of $\{\mathcal{U}_i\}$ in equation (18) into multiple PSD constraints of \mathbf{S}_+^{18} each. This approach roughly corresponds to the so-called ‘edge based relaxation’ techniques for SDP and allows us to utilise qE -NRSfM for problems with a moderate number of point correspondences. Since SDP has an arithmetic operation complexity of $\mathcal{O}(n^3)$, splitting into smaller matrices accelerates the solution significantly. Concretely, we do this in two steps.

Auxiliary variable. As the *first* step, we introduce the auxiliary variable $\mathfrak{V}_i = \mathfrak{Q}'_i(\mathfrak{Q}'_i)^\top$, such that $\mathfrak{Q}'_i = \left(\vartheta(i, j, q)^\top, \vartheta(i, q, r)^\top, \vartheta(i, j, r)^\top, \dots \right)^\top$. \mathfrak{V}_i allows us to split \mathcal{U}_i into: 1) \mathfrak{V}_i , and 2) \mathfrak{S}'_i (once again). Therefore, equation (18) modifies to:

$$\min_{\{\mathfrak{S}'_i\}, \{\mathfrak{V}_i\}, \mathcal{G}_2, \mathcal{G}_3} \sum_{i=1}^n \left(\left(f_{i,j}^\Pi(\mathfrak{S}'_i) + \text{tr}(\mathfrak{S}'_i) + \text{tr}(\mathfrak{V}_i) \right) + \sum_{j,q=1}^{m, \mathcal{E}_2(j)} \left(\lambda_I |\mathfrak{g}_I^P(i, j, q) - \mathcal{G}_2(j, q)| - f_{i,j}^\delta(\mathfrak{S}'_i) + \sum_{r=1}^{\mathcal{E}_3(j,q)} \lambda_E |\mathfrak{g}_E^P(i, j, q, r) - \mathcal{G}_3(j, q, r)| \right) \right) \quad (8a)$$

$$\text{s.t. } (\mathfrak{S}'_{i,j,q})^2 \leq \mathfrak{V}_{i,b'_t,b'_t}, \sum_{j,q=1}^{m, \mathcal{E}_2(j)} \mathcal{G}_2(j, q) = 1, \mathfrak{S}'_{i,1,1} = 1, \\ \mathfrak{S}'_i \in \mathbf{S}_+^{3m+1}, \quad \mathfrak{V}_i \in \mathbf{S}_+^{6\tilde{p}_2}, \quad b'_t = b_t - (3m + 1) \\ \forall \quad b_t \in \rho^k(j, q, r), t \in [1, 18], i \in [i, n], \\ j \in [1, m], (j, q) \in \mathcal{E}_2, (j, q, r) \in \mathcal{E}_3, \lambda_I > 0, \quad (8b)$$

Principal sub-matrices. The *second* modification comes from the principal sub-matrices of \mathfrak{V}_i . Following our strategy to limit usage of PSD constraints to smaller matrices, we extract those principal sub-matrices of \mathfrak{V}_i which represents the 18×18 matrix of the edges of each 2-simplex in \mathcal{E}_3 . For doing this, we define a map β^k such that:

$$\beta_{j,q,r}^k(\mathfrak{V}_i) = \begin{pmatrix} \vartheta(i, j, q)^\top \\ \vartheta(i, q, r)^\top \\ \vartheta(i, j, r)^\top \end{pmatrix}^\top \begin{pmatrix} \vartheta(i, j, q)^\top \\ \vartheta(i, q, r)^\top \\ \vartheta(i, j, r)^\top \end{pmatrix} \in \mathbb{R}^{18 \times 18} \quad (9)$$

This allows us to re-write equation (8) with smaller PSD constraints, given by:

$$\min_{\{\mathfrak{S}'_i\}, \{\mathfrak{V}_i\}, \mathcal{G}_2, \mathcal{G}_3} \sum_{i=1}^n \left(\left(f_{i,j}^\Pi(\mathfrak{S}'_i) + \text{tr}(\mathfrak{S}'_i) + \text{tr}(\mathfrak{V}_i) \right) + \right.$$

$$\sum_{j,q=1}^{m, \mathcal{E}_2(j)} \left(\lambda_I |\mathfrak{g}_I^P(i, j, q) - \mathcal{G}_2(j, q)| - f_{i,j}^\delta(\mathfrak{S}'_i) + \sum_{r=1}^{\mathcal{E}_3(j,q)} \lambda_E |\mathfrak{g}_E^P(i, j, q, r) - \mathcal{G}_3(j, q, r)| \right) \quad (10a)$$

$$\text{s.t. } (\mathfrak{S}'_{i,j,q})^2 \leq \mathfrak{V}_{i,b'_t,b'_t}, \sum_{j,q=1}^{m, \mathcal{E}_2(j)} \mathcal{G}_2(j, q) = 1, \mathfrak{S}'_{i,1,1} = 1, \\ \mathfrak{S}'_i \in \mathbf{S}_+^{3m+1}, \quad \beta_{j,q,r}^k(\mathfrak{V}_i) \in \mathbf{S}_+^{18}, \quad b'_t = b_t - (3m + 1) \\ \forall \quad b_t \in \rho^k(j, q, r), t \in [1, 18], i \in [i, n], \\ j \in [1, m], (j, q) \in \mathcal{E}_2, (j, q, r) \in \mathcal{E}_3, \lambda_I > 0. \quad (10b)$$

5. Simulators

We use two simulators, one for generating randomly deforming isometric surfaces and another for generating randomly deforming equiareal surfaces. We describe these two simulator below.

Isometric surfaces. The ISG proposed by us is based on the method of [10]. Given a sparse grid of $m_a \times m_b$ flat 3D points $\mathbf{T}_s \in \mathbb{R}^{3 \times m}$ (with $m = m_a m_b$), we use the model from [10] to create n bounded developable surfaces, represented as a pointcloud $\{\mathbf{P}_{S,i} \in \mathbb{R}^{3 \times m}, \forall i \in [1, n]\}$. This is done by assigning random bending angles to the rulings used to map \mathbf{T}_s to $\{\mathbf{P}_{S,i}\}$ using [10]. To $\{\mathbf{P}_{S,i}\}$, we assign random roto-translations $\mathbf{R}_{S,i}, \mathbf{t}_{S,i}$ and perspectively project to $\{\mathbf{p}_{S,i}\}$ using random realistic camera intrinsics. Optionally, we modify each projected point $\mathbf{p}_{S,i,j}$ by adding noise $\mathbf{p}'_{S,i,j} = \mathbf{p}_{S,i,j} + x_\sigma \sigma_1$, where $\sigma_1 \sim \mathcal{U}(0, 1)$ is drawn from a random uniform distribution and the parameter x_σ is a scalar multiplier. $\{\mathbf{p}'_{S,i}\}$ gives our *isometric simulated* data from ISG.

Equiareal surfaces. For our $qESG$, we follow the same framework as ISG, but randomly deform the developable surfaces $\{\mathbf{P}_{S,i}\}$ and use non-linear least squares to enforce equal area between 2-simplices. Given $\{\mathbf{P}_{S,i}\}$ from \mathbf{T}_s using [10], we obtain each randomly deformed 3D point as $\mathbf{P}_{E,i,j} = \mathbf{P}_{S,i,j} + \mathbf{1} \chi_e \sigma_2$, where $\sigma_2 \sim \mathcal{U}(-0.5, 0.5)$ is drawn from a random uniform distribution and $\mathbf{1} = (1, 1, 1)$. We already have \mathcal{G}_3 from \mathbf{T}_s . Therefore, the quasi-equiareal pointcloud is obtained as:

$$\{\mathbf{P}_{Q,i}\} = \underset{\{\mathbf{P}_{E,i,j}\}}{\text{argmin}} \sum_{i,j,q,r=1}^{n, m, \mathcal{E}_2(j), \mathcal{E}_3(j,q)} \left(\mathcal{G}_3(j, q, r) - \mathfrak{g}_E(i, j, q, r) \right)^2. \quad (11)$$

We solve equation (11) with the Levenberg–Marquardt algorithm.

6. Additional Experimental Results

We now present some additional results that could not be included in the main article due to space limitations:

6.1. Additional qualitative results





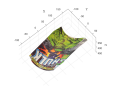
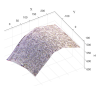
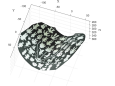
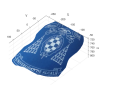
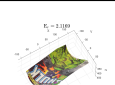
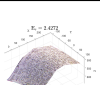
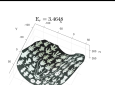
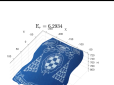
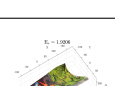
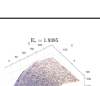
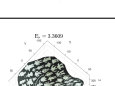
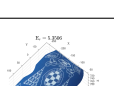
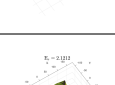
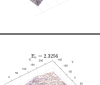
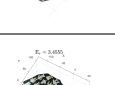
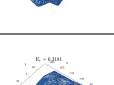
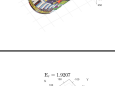
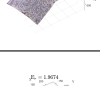
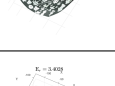
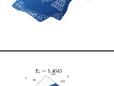
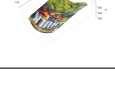
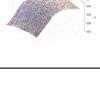


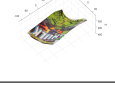
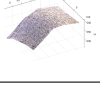
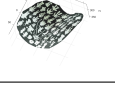
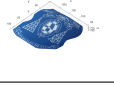
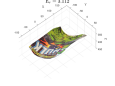
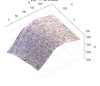
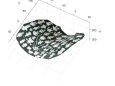
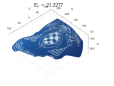
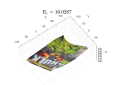
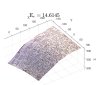
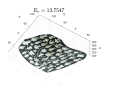
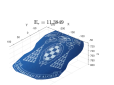
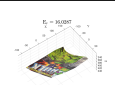
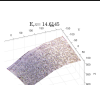
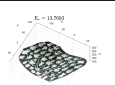
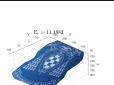
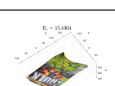
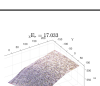
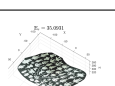
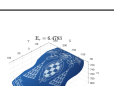
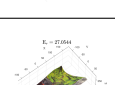
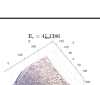
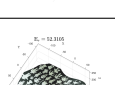
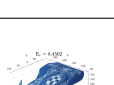
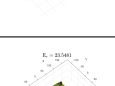
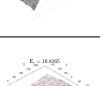
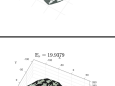
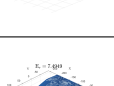
We show some qualitative results from our experiments on the Hulk, KP, WC and ST datasets with $sI-\delta$, $sI-P$, $qI-\delta$ and $qI-P$ in table (2). We show one frame for each of the datasets, densely interpolated using [1]. Our proposed methods reconstruct the shape accurately in all cases. Among the state-of-the-art methods, the zeroth order NRSfM techniques ([3], [8]) are very accurate with the inextensible objects (KP, WC, Hulk), but we manage to outperform them in KP and Hulk, while in WC, we are the close second. LRSB methods ([7], [6], [4]) do not seem to be very accurate with inextensible objects. However, in the highly extensible data of ST, the LRSB methods work very accurately, the zeroth order methods suffer to maintain accuracy and our proposed method maintains accuracy at par with LRSB methods. These results on these datasets fit the claim that quasi-isometry is a better model for handling both inextensible and extensible objects, which is not the case for either the previous zeroth-order NRSfM methods or the LRSB methods. In figure (4), we show some additional qualitative results on synthetic data using $sI-\delta$, $sI-P$, $qI-\delta$ and $qI-P$ on ISG.

Next we show some qualitative results from our experiments on SB and SL with $eI-\delta$. The qualitative results from a sample frame of each dataset is shown in table (3). SB is a highly curved surface of a balloon being sheared by compressive force. All methods except $eI-\delta$ fails to recover the curvature of the balloon, this is clearly observable in the qualitative results. On the other hand, SL is a rectangular patch from a nearly-planar surface of a highly stretched leggings. While most of the compared methods, except [8], reconstructs the surface reasonably accurately, [2], [7] and [3] reconstructs a mildly curved surface, which is not similar to Gt . In the example of SL shown in table (3), $qI-\delta$ is already more accurate than the other methods, while $eI-\delta$ improves the accuracy, over and above what is achieved by quasi-isometry.

6.2. Effect of sparsity on accuracy of $eI-\delta$

In the main article, we had briefly talked about the effect of sparsity on accuracy of $eI-\delta$. A non-chordal PSD matrix completion without additional measures for handling sparsity can lead to sub-optimal solutions [5]. Unfortunately, for denser correspondences, maintaining a fully connected graph structure via \mathcal{E}_3 lead to extremely large $\{\mathcal{T}_i\}$, which is computationally infeasible. We show this via a small-scale, synthetic example in figure (3). As we increase the number of point correspondences in the input data while maintain-

Table 2. Qualitative results for Hulk, KP, WC, ST

	Hulk	KP	WC	ST
Input				
Gt				
$sI-\delta$				
$sI-P$				
$qI-\delta$				
$qI-P$				
[8]				
[3]				
[9]-IP				
[9]-G				
[7]				
[6]				
[4]				
[2]				

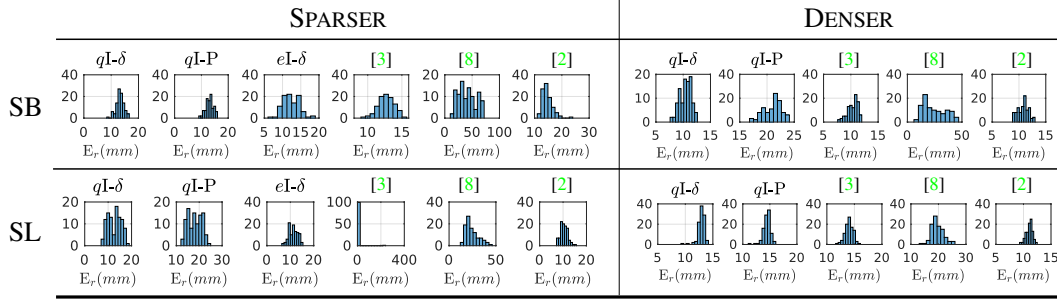


Figure 2. The sparser plots are obtained by repeatedly and sparsely subsampling a set of large correspondences while the denser plots are obtained by densely subsampling the same set of large correspondences

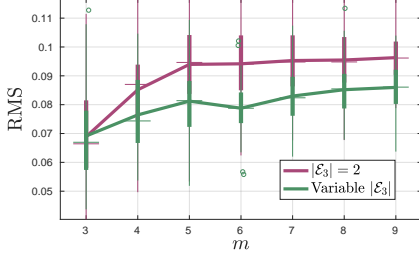


Figure 3. Variation of accuracy with sparsity with two different strategies: one with a constant \mathcal{E}_3 of two 2-simplices and the other creates a nearly chordal graph-structure with adaptive \mathcal{E}_3

ing a constant $|\mathcal{E}_3|$ of 2, the accuracy decreases with increasing density, as the number of cliques in $\{\mathcal{T}_i\}$ increases. In such a case, there can certainly exist situations where $sI-\delta$ or $sI-P$ dominates in accuracy over $eI-\delta$. However, this decrease in accuracy can be compensated by adapting $|\mathcal{E}_3|$, such that $\{\mathcal{T}_i\}$ remains fully connected, as shown in figure (3). But this is not generalisable to actual, larger dataset with large point correspondences due to computational limitations. Notably, such an effect of sparsity is absent in $sI-\delta$, $sI-P$, $qI-\delta$ or $qI-P$, since arbitrarily increasing neighborhood does not create a significant computational bottleneck for these methods.

However, in figure (2), we show that for the two extensible objects SL and SB, the higher accuracy of $eI-\delta$ (from Table 2) is generalisable to different correspondences across multiple resolutions. We randomly sample ~ 50 point correspondences from SB and SL in two different resolutions, the *sparser* one being 11 correspondences and the *denser* one being ~ 30 points. Over many repetitions, we show that $eI-\delta$ with sparser correspondences form the most accurate method of reconstruction over all resolutions, although the accuracy improvement over [2, 3] are relatively small. But importantly, there is a significant and consistent improvement in accuracy with $eI-\delta$ over $qI-\delta$, which fits our goal of obtaining a $qE-NRSfM$ method that improves upon our proposed $qI-NRSfM$ in case of highly stretchable objects.

6.3. Results from $eI-P$

With the modification to $eI-P$ from equation (10), the E_r on SB and SL are 12.48 and 8.35 mm respectively, while the qualitative results have been shown along with other methods in table (3). In comparison with table (2) of the main paper, $eI-P$ appears less accurate than $eI-\delta$. This is surprising, since in most experiments, $p3D$ methods seem to outperform $DaSL$ methods. But for $eI-P$, this drop in accuracy stems from the additional relaxations of section (4). However, $eI-P$ nonetheless marginally improves the results of $qI-P$.

References

- [1] Isaac Amidror. Scattered data interpolation methods for electronic imaging systems: a survey. *Journal of electronic imaging*, 11(2):157–176, 2002. 5
- [2] Ajad Chhatkuli, Daniel Pizarro, and Adrien Bartoli. Non-rigid shape-from-motion for isometric surfaces using infinitesimal planarity. In *BMVC*, 2014. 5, 6, 8
- [3] Ajad Chhatkuli, Daniel Pizarro, Toby Collins, and Adrien Bartoli. Inextensible non-rigid structure-from-motion by second-order cone programming. *IEEE transactions on pattern analysis and machine intelligence*, 40(10):2428–2441, 2017. 2, 5, 6, 8
- [4] Yuchao Dai, Hongdong Li, and Mingyi He. A simple prior-free method for non-rigid structure-from-motion factorization. *International Journal of Computer Vision*, 107(2):101–122, 2014. 5
- [5] Mitsuhiro Fukuda, Masakazu Kojima, Kazuo Murota, and Kazuhide Nakata. Exploiting sparsity in semidefinite programming via matrix completion i: General framework. *SIAM Journal on optimization*, 11(3):647–674, 2001. 5
- [6] Paulo FU Gotardo and Aleix M Martinez. Kernel non-rigid structure from motion. In *2011 International Conference on Computer Vision*, pages 802–809. IEEE, 2011. 5, 8
- [7] Onur C Hamsici, Paulo FU Gotardo, and Aleix M Martinez. Learning spatially-smooth mappings in non-rigid structure from motion. In *European Conference on computer vision*, pages 260–273. Springer, 2012. 5, 8
- [8] Pan Ji, Hongdong Li, Yuchao Dai, and Ian Reid. "maximizing rigidity" revisited: a convex programming approach for

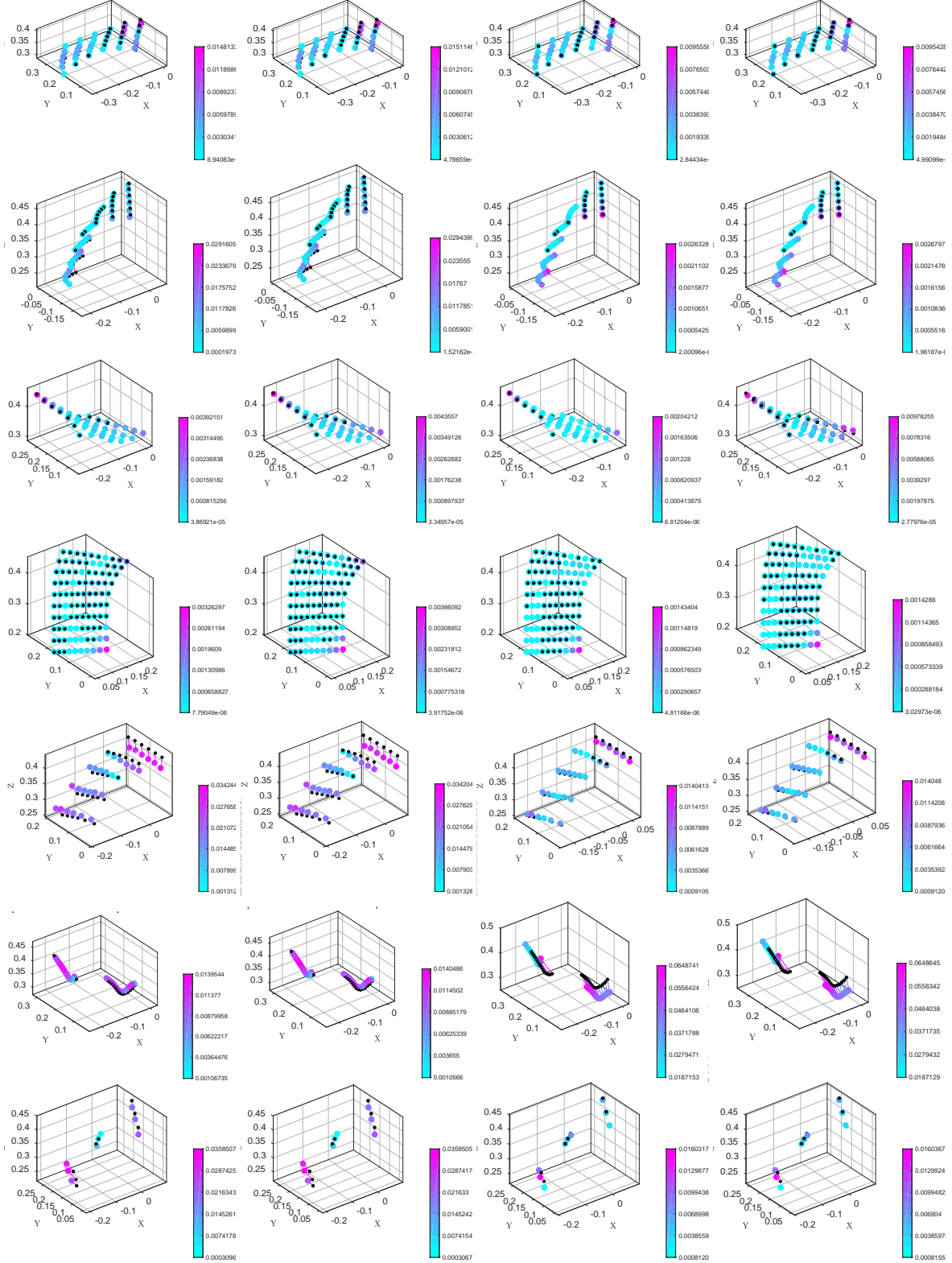


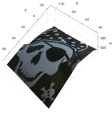
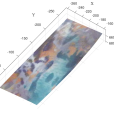
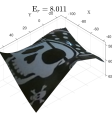
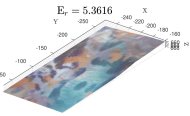
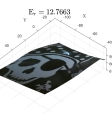
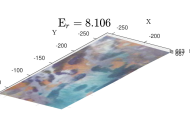
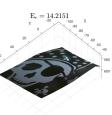
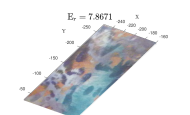
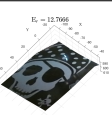
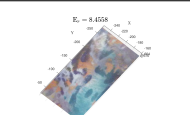
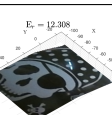
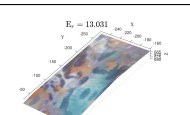
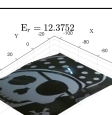
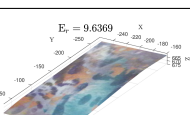
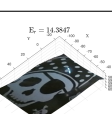
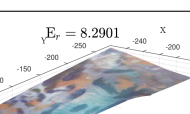
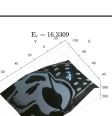
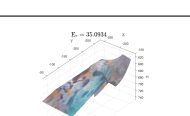
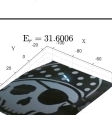


Figure 4. We show some demonstrative synthetic results from ISG with four of our isometric methods. Each row represents a new dataset. The *first* column is $sI-\delta$, the *second* column is $qI-\delta$, the *third* column is $sI-P$ and the *fourth* column is $qI-P$. Black points are G_t and the reconstructed points are color-coded by their Euclidean distance to corresponding G_t point (connected by a thin line). All units in au

Table 3. Results on SB and SL (‘×’ for methods that failed)

	SB	SL
Input		
Gt		
$eI-\delta$		
$eI-P$		
$qI-\delta$		
$qI-P$		
[2]		
[7]		
[3]		
[8]		
[6]		×

generic 3d shape reconstruction from multiple perspective views. In *Proceedings of the IEEE International Conference on Computer Vision*, pages 929–937, 2017. [2](#), [5](#), [6](#), [8](#)

- [9] Shaifali Parashar, Daniel Pizarro, and Adrien Bartoli. Isometric non-rigid shape-from-motion with riemannian geometry solved in linear time. *IEEE transactions on pattern analysis and machine intelligence*, 40(10):2442–2454, 2017. [5](#)
- [10] Mathieu Perriollat and Adrien Bartoli. A computational model of bounded developable surfaces with application to image-based three-dimensional reconstruction. *Computer Animation and Virtual Worlds*, 24(5):459–476, 2013. [4](#)
- [11] Zizhuo Wang, Song Zheng, Yinyu Ye, and Stephen Boyd. Further relaxations of the semidefinite programming approach to sensor network localization. *SIAM Journal on Optimization*, 19(2):655–673, 2008. [3](#)